Finite element model updating and damage identification using semi-rigidly connected frame element and optimization procedure: An experimental validation

Parsa Ghannadi [1], Samir Khatir [2], Seyed Sina Kourehli [3], Andy Nguyen [4], Djilali Boutchicha [5], and Magd Abdel Wahab *[2]

[1] *Department of Civil Engineering, Ahar Branch, Islamic Azad University, Ahar, Iran*

[2] *Soete Laboratory, Faculty of Engineering and Architecture, Ghent University, Technologiepark Zwijnaarde 903, B-9052 Zwijnaarde, Belgium*

[3] *Department of Civil Engineering, Azarbaijan Shahid Madani University, Tabriz, Iran*

[4] *School of Engineering, University of Southern Queensland, Springfield, QLD 4300, Australia*

[5] *Laboratoire de Mécanique Appliquée, Université des Sciences et de la Technologie d'Oran - Mohamed Boudiaf, Algeria*

* Corresponding author: Magd.AbdelWahab@UGent.be (Magd Abdel Wahab)

Abstract. Owing to ever-increasing complexity of engineering structures, developing a methodology for the early detection of defects has become crucial to ensure their long-term safety and reliability with the least amount of expense. There are always discrepancies between experimental and numerical modal data because of unknown structural parameters and uncertainties. The finite element model (FEM) updating techniques attempt to minimize the differences by adjusting the unknown parameters of the FEM. Therefore, the FEM updating methods are essential for developing a baseline model and accurate damage identifications in subsequent steps. This paper employs the semi-rigidly connected frame element (S-RCFE) instead of the standard Euler-Bernoulli beam element for assembling the FEM of the experimental beam and establishing a high-fidelity numerical model. The S-RCFE with extra design parameters, including the end fixity factor of all connections, enables us to achieve a reasonable agreement between experimental and numerical models through the optimization-based procedure. In FEM updating step, two objective functions based on modified total modal assurance criterion (MTMAC) and changes in natural frequency are used to minimize by three optimization algorithms, viz, grey wolf optimizer (GWO), gradient-based optimization (GBO), and an improved version of GWO (IGWO). The influence of the S-RCFE and standard Euler-Bernoulli beam on the model updating accuracy is also examined, and the efficiency of S-RCFE is evaluated. The statistical results reveal that GWO-MTMAC and IGWO-MTMAC can be successfully implemented for FEM updating with almost the same performance. However, IGWO provides the most reliable results with a relatively extensive computation time for damage identification in all scenarios. In some damage scenarios, the GWO and GBO perform comparably with very similar running time.

Keywords: Damage identification, Semi-rigidly connected frame element, Euler-Bernoulli beam element, Grey wolf optimizer, Gradient-based optimization, Modified total modal assurance criterion, Experimental beam

1. Introduction

Civil asset owners often prioritise civil structure safety more than anything else since it directly impacts human lives [1]. In engineering structures like highrise buildings, bridges, tunnels, and dams, undetected changes in operational conditions can result in cumulative damage [2, 3]. These structures are susceptible to severe damage and potentially catastrophic failure if initial damage is not promptly discovered [4, 5]. These structures, especially the older ones, need to be monitored so that any damage can be found early. The essential retrofitting can be done to ensure they can remain operational safely and reliably without unexpected breakdowns [6]. Structural health monitoring (SHM) induces beneficial knowledge about a structure's function by analyzing responses, identifying damage, and assessing the present condition [7].

According to Farrar et al. [8], the aims of the SHM strategy are classified into five levels. The first level is related to recognizing the presence of damages. The second to fourth levels are designed to report the location, type, and severity of damaged elements, respectively, whereas the last level gives information on the building's safety. To find the damaged elements and quantify their severities in model-based methods, researchers propose inverse analysis to compare the actual structural response with calculated responses from the numerical model during an optimization procedure [9]. However, the ill-posed inverse problem [10] appears in some indicators when one structural response may correspond to complete damage parameters. Robust optimization algorithms are well placed to solve this problem by exploring the search space and preventing the local solutions. The inverse analysis can be very computationally demanding [11], as it requires the simulation of the problem several times in each iteration. In metaheuristic algorithms, several times means a value equivalent to the population size. Therefore, employing a proper optimization algorithm is critical regarding computational cost. Moreover, the performance of optimization algorithms is guided by their control parameters, such as probabilities of crossover and mutation in the genetic algorithm [12]. However, the Jaya algorithm does not contain control parameters, making it flexible in solving various engineering problems [13]. The population size and the maximum number of iterations are only two algorithmic parameters for beginning optimization with the Jaya algorithm [14]. Although a smaller population increases convergence speed, it also increases the risk of trapping in local optima [15]. Overall, each problem requires specific tuning of these parameters to take full advantage of the algorithm potential [16]. Several studies have been conducted to date regarding the flexible and successful application of the Jaya algorithm for structural damage identification [11, 17, 18]. Additionally, for crack identification in plate structures, Khatir and

Wahab demonstrated the advantage of the Jaya algorithm in terms of accuracy and convergence rate compared to particle swarm optimization (PSO) [19]. Another optimization algorithm without control parameters is teaching-learning-based optimization (TLBO). Similar to the Jayal algorithm, algorithmic parameters are required to operate [20]. In recent years, TLBO has been extensively applied for different engineering problems such as structural damage identification [20-23]. Due to the limited number of sensors, measuring entire mode shapes from the experiment is not always practical [24]. Therefore, Das and Dhang [25] presented a damage detection method for frame and truss structures utilizing an improved version of TLBO-PSO and iterated improved reduction system (IIRS). Model reduction techniques condense the degrees of freedom (DOFs) of the finite element model to match the measured DOFs [26, 27]. For further study, the accuracy of several finite element model (FEM) reduction strategies was studied by Ghannadi and Kourehli [28]. Dinh-Cong et al. performed a comparative study of different dynamic condensation techniques for optimization-based damage identification of plate-like structures [29]. Numerous attempts exist to combine the different optimization algorithms and model reduction techniques for damage identification, such as IIRS and lightning attachment procedure optimization [30], IIRS and PSO-gravitational search algorithm [31], second-order Neumann series expansion and adaptive hybrid evolutionary firefly algorithm [32]. Another strategy to address the challenge of limited measurements is the mode shape expansion method, which expands the experimental mode shapes to meet the FEM [33, 34]. Au et al. presented one of the earliest methodologies that integrate the system equivalent reduction expansion process (SEREP) and micro GA for damage detection [35]. After developing robust nature-inspired optimization algorithms, Ghannadi and Kourehli [36] introduced a damage identification method based on the grey wolf optimizer (GWO) and SEREP. In another study for damage assessment in three-dimensional structures, the SEREP is employed to estimate all DOFs. Then, the discrepancy between measured and calculated mode shapes is minimized to solve the optimization problem through the steepest descent method [37].

The objective function is crucial for updating structural model parameters and successfully determining damage elements and severity [38]. Therefore, numerous objective functions have been developed and implemented for various damage detection problems [39]. For example, Ghannadi and Kourehli suggested a hybrid objective function based on modal assurance criterion flexibility and natural frequency for minimizing by moth-flame optimization [40]; Ding et al. proposed a new cost function relying on natural frequencies, mode shapes, and an

$L_{0.5}$ regularization for beginning optimization procedure via an improved version on Jaya algorithm [41]; Pahnabi and Seyedpoor formulated an objective function using the nodal acceleration vectors [42]; Tiachacht et al. implemented a strategy based-on modal strain energy change ratio and two optimizers including slime mould algorithm and marine predators algorithm [43]; Ghannadi and Kourehli applied different kinds of objective functions such as modified total modal assurance criterion (MTMAC), modal assurance criterion (MAC) [44, 45] and natural frequency vector assurance criterion [46].

Several researchers studied the performance of hybridization of artificial neural networks (ANNs) and optimization algorithms for presenting efficient damage detection method. For instance, Tran-Ngoc et al. [47] combined the ANNs and PSOGA by using the stochastic search capability of PSOGA to control the ANNs from entrapping in local minima; Nguyen-Ngoc et al. [48] employed the PSO to optimize the training parameters (weight and bias) of ANNs; in another study conducted by Khatir et al. [49], the Jaya algorithm was applied to find the most optimal values for training parameters of ANNs.

To obtain accurate results in real-world damage detection problems, precise model updating strategy and calibrating the numerical model to describe the actual behavior of the structure is the most critical issue. The uncertain parameters, including Young's modulus [50, 51]; Young's modulus and mass density [52]; Young's modulus and spring stiffness [53]; stiffness coefficients [54]; linear density, flexural rigidity, torsion spring coefficient and vertical spring coefficient [55], have routinely been selected by previous studies. However, the mentioned research could not provide the most accurate FEM strategy, and there are differences between experimental and updated natural frequencies. Additionally, the fidelity of the updated model is usually decreased at the higher modes. The semi-rigidly connected frame element (S-RCFE) with additional design parameters such as end fixity factors enables us to achieve exact solutions during the optimization-based FEM updating procedure. The S-RCFE is the generalized form of the Euler-Bernoulli beam element, initially developed to represent the semi-rigid connections in steel frames. Several researchers have introduced the optimization-based method to joint damage detection with the contribution of the S-RCFE [42, 56-59]. To the best of the authors' knowledge, no studies in the literature consider the end fixity factors and Young's modulus as design parameters in FEM updating.

Prompted by these limitations, this paper investigates how developed FEM based on S-RCFE influences the accuracy of the model updating procedure. Moreover, the sensitivity of two objective functions based on MTMAC and changes in natural frequency are analyzed through

statistical investigations, including mean and standard deviation in identifications. In addition, this study employs the improved GWO (IGWO) to address the imbalance between exploration and exploitation, the lack of population diversity, and the premature convergence of standard GWO [60]. The performance of IGWO in terms of convergence rate, computation time, and stability of results for different independent runs is compared to standard GWO and a newly developed algorithm called gradient-based optimizer (GBO).

The rest of the paper is structured as follows: Section 2 presents the methodology of the inverse crack detection method, including stiffness and mass matrices of the S-RCFE for assembling the FEM, objective functions and uncertain parameters for FEM updating, and structural damage definition. The mathematical formulations of utilized optimization algorithms, including GWO, IGWO, and GBO, are briefly described in Section 3. Section 4 explains the free-free beam's experimental setup and measured vibration characteristics. The results and discussion are provided in Section 5. The paper is finally summarized in Section 6.

2. Methodology

This section presents the mathematical formulations of utilized FEM for simulating structures with semi-rigid joints, the FEM updating procedure with employed objective functions, the definition of structural damages, and the suggested inverse method for their identification.

2.1. Local stiffness and mass matrices for semi-rigid connected elements

Most joints in frame structures are actually semi-rigid, which means that depending on the fixity factor, they can rotate to a certain degree. The end fixity factor has a theoretical range of 0 to 1, with a value of zero denoting an entirely hinged joint and a value of 1 indicating an utterly rigid joint. The most typical technique to describe semi-rigid connections is as infinitesimally short rotating springs hooked to the beam's ends [58, 61], as seen in Figure 1. In this paper, the semi-rigidly connected frame element (S-RCFE) is adopted instead of the Euler-Bernoulli beam element to assemble a FEM of a free-free beam. In reality, the behavior of beam-like structures is considered perfectly rigid without any connections. However, using the S-RCFE with extra design parameters such as end fixity factors allows us to update the FEM accurately through the optimization-based procedure.

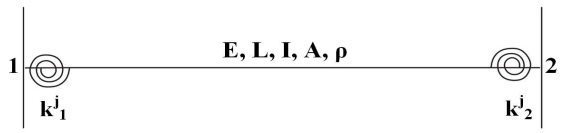

Figure 1. The semi-rigidly connected frame element with rotational stiffness k^j

The following equation provides the stiffness matrix for the semi-rigidly connected frame element [58, 61]:

$$[k]=\frac{EI}{L}\begin{bmatrix} \frac{A}{I} & 0 & 0 & -\frac{A}{I} & 0 & 0 \\ 0 & \frac{4(\alpha_1+\alpha_2+\alpha_3)}{L^2} & \frac{2(2\alpha_1+\alpha_2)}{L} & 0 & -\frac{4(\alpha_1+\alpha_2+\alpha_3)}{L^2} & \frac{2(2\alpha_2+\alpha_3)}{L} \\ 0 & \frac{2(2\alpha_1+\alpha_2)}{L} & 4\alpha_1 & 0 & -\frac{2(2\alpha_1+\alpha_2)}{L} & 2\alpha_2 \\ -\frac{A}{I} & 0 & 0 & \frac{A}{I} & 0 & 0 \\ 0 & -\frac{4(\alpha_1+\alpha_2+\alpha_3)}{L^2} & -\frac{2(2\alpha_1+\alpha_2)}{L} & 0 & \frac{4(\alpha_1+\alpha_2+\alpha_3)}{L^2} & -\frac{2(\alpha_2+2\alpha_3)}{L} \\ 0 & \frac{2(2\alpha_2+\alpha_3)}{L} & 2\alpha_2 & 0 & -\frac{2(\alpha_2+2\alpha_3)}{L} & 4\alpha_3 \end{bmatrix} \tag{1}$$

where the following equation calculates a_1, a_2, and a_3:

$$\left.\begin{aligned} \alpha_1 &= \frac{3J_1}{4-J_1J_2} \\ \alpha_2 &= \frac{3J_1J_2}{4-J_1J_2} \\ \alpha_3 &= \frac{3J_2}{4-J_1J_2} \end{aligned}\right\} \tag{2}$$

where J_1 and J_2 indicate the end fixity factors for joint 1 and joint 2, respectively.

The mass matrix for the semi-rigidly connected frame element is given by the following equation:

$$[m]=\frac{\rho AL}{420D^2}\begin{bmatrix} 140D^2 & 0 & 0 & 70D^2 & 0 & 0 \\ 0 & 4f_1 & 2Lf_2 & 0 & 2f_3 & -Lf_4 \\ 0 & 2Lf_2 & 4L^2f_5 & 0 & Lf_4 & -L^2f_6 \\ 70D^2 & 0 & 0 & 140D^2 & 0 & 0 \\ 0 & 2f_3 & Lf_4 & 0 & 4f_1 & -2Lf_2 \\ 0 & -Lf_4 & -L^2f_6 & 0 & -2Lf_2 & 4L^2f_5 \end{bmatrix} \tag{3}$$

where the parameters $D, f_1, f_2, f_3, f_4, f_5$, and f_6 are determined based on the end fixity factors as follows:

$$\left.\begin{aligned} D &= 4-J_1J_2 \\ f_1 &= 560+224J_1+32J_1^2-196J_2-328J_1J_2-55J_1^2J_2+32J_2^2+50J_1J_2^2+32J_1^2J_2^2 \\ f_2 &= 224J_1+64J_1^2-160J_1J_2-86J_1^2J_2+32J_1J_2^2+25J_1^2J_2^2 \\ f_3 &= 560-28J_1-64J_1^2-28J_2-184J_1J_2+5J_1^2J_2-64J_2^2+5J_1J_2^2+41J_1^2J_2^2 \\ f_4 &= 392J_2-100J_1J_2-64J_1^2J_2-128J_2^2-38J_1J_2^2+55J_1^2J_2^2 \\ f_5 &= 32J_1^2-31J_1^2J_2+8J_1^2J_2^2 \\ f_6 &= 124J_1J_2-64J_1^2J_2-64J_1J_2^2+31J_1^2J_2^2 \end{aligned}\right\} \tag{4}$$

2.2. Dynamic characteristics

The following eigenvalue equation is used to compute the dynamic properties [62], such as the i^{th} natural frequencies and the corresponding mode shapes:

$$K\phi_i = \omega_i^2 M\phi_i, \qquad i=1, 2, \ldots, n \tag{5}$$

where K and M denote the stiffness and mass matrices, respectively. ϕ_i is the i^{th} mode shape vector, and ω_i is the i^{th} natural frequency. n symbolizes the number of DOFs.

2.3. Optimization-based FEM updating procedure

Real-world applications reveal notable differences between numerical estimations and measurements, regardless of the proper capability of FEM for characterizing the dynamic behavior of structures. These differences are predominantly caused by uncertain boundary conditions, imprecise material parameters, and uncertainties regarding geometry configuration [63, 64]. As a result, numerous techniques for addressing the inverse problems of FEM updating have been developed. The methods based on the minimization of objective function through optimization algorithms have received incredible attention due to their accuracy and relatively fast computation time. As mentioned in the introduction section, the objective function plays an undeniable role in accurately model updating and finalizing a high-fidelity numerical model for the subsequent usage in the damage identification step. Therefore, two objective functions based on MTMAC [44] and natural frequency [51] are adopted to conduct the statistical investigations for FEM updating. The MTMAC is an efficient objective function that integrates MAC and natural frequencies to satisfy both updating criteria in terms of mode shapes and natural frequencies [65, 66]. In this paper, Young's modulus of all elements and the end fixity factor of all joints are assumed as uncertain parameters (X) in the model updating procedure. According to Eq. (1), there is a direct association between Young's modulus and stiffness matrix. Therefore, uncertainties in elemental stiffness matrices are quantified by tuning Young's modulus of each element. Additionally, Young's modulus is sensitive to temperature changes [67-69], which can be caused uncertainty.

$$f_{MTMAC}(X) = \left(\sum_{i=1}^{n} \left(1 - MTMAC_i(X)\right) \right) \tag{6}$$

where:

$$MTMAC_i(X) = \frac{MAC_i\left(\{\phi_i^m\},\{\phi_i^c(X)\}\right)}{1+\left|\frac{\left(\omega_i^m\right)^2-\left(\omega_i^c(X)\right)^2}{\left(\omega_i^m\right)^2+\left(\omega_i^c(X)\right)^2}\right|} \tag{7}$$

where $\omega_i^c(X)$ and ω_i^m demonstrate the i^{th} calculated and measured natural frequencies, and the MAC value between two mode shape vectors is calculated as follows:

$$MAC_i(X) = \frac{\left|\{\phi_i^m\}^T\{\phi_i^c(X)\}\right|^2}{\left(\{\phi_i^c(X)\}^T\{\phi_i^c(X)\}\right)\left(\{\phi_i^m\}^T\{\phi_i^m\}\right)} \tag{8}$$

$$f_{frequency}(X) = \sum_{i=1}^{n}\left(\left(\omega_i^m-\omega_i^c(X)\right)^2/\left(\omega_i^m\right)^2\right) \tag{9}$$

2.4. Damage definition

Different defects such as cracks, holes, and abrasion generally induce a certain percent of stiffness reduction in elements [70]. The changes in the elemental stiffness of the structure are represented by the stiffness reduction factor (SRF). The damaged stiffness matrix K_d is defined based on the SRF by the following equation [71]:

$$K_d = \sum_{e=1}^{N}(1-SRF_e)k_e \tag{10}$$

where SRF_e stands for the e^{th} stiffness reduction factor, ranging from 0 to 1, while 0 denotes the undamaged condition and 1 indicates a severely damaged state. The number of elements and e^{th} local stiffness matrix is also shown by N and k_e, respectively.

2.5. Optimization-based damage detection procedure

Dynamic characteristics change as structures experience damage. Because of this, various vibration-based inverse techniques have been proposed to identify structural deterioration using changes in structural vibration characteristics [72]. Mode shapes and their derivatives as a fundamental component for damage identification have significant advantages over natural frequencies. However, the drawbacks are also prominent. For instance, the mode shapes must be measured using a series of sensors, and they are also more sensitive to noise contamination than natural frequencies [73]. Therefore, employing a damage detection strategy with the advantage of using only the first few natural frequencies without the mode shape components is applicable in real-world damage identification problems [74]. The following objective function relying on changes in natural frequencies is applied to minimize

by the optimization algorithms, including GWO, IGWO, and GBO.

$$f_{frequency}\left(SRF_e\right)=\sum_{i=1}^{n}\left(\left(\omega_i^m-\omega_i^c\left(SRF_e\right)\right)^2/\left(\omega_i^m\right)^2\right),\qquad 0\le SRF_e\le 1 \tag{11}$$

Figure 2 displays the flowchart of the proposed damage detection strategy.

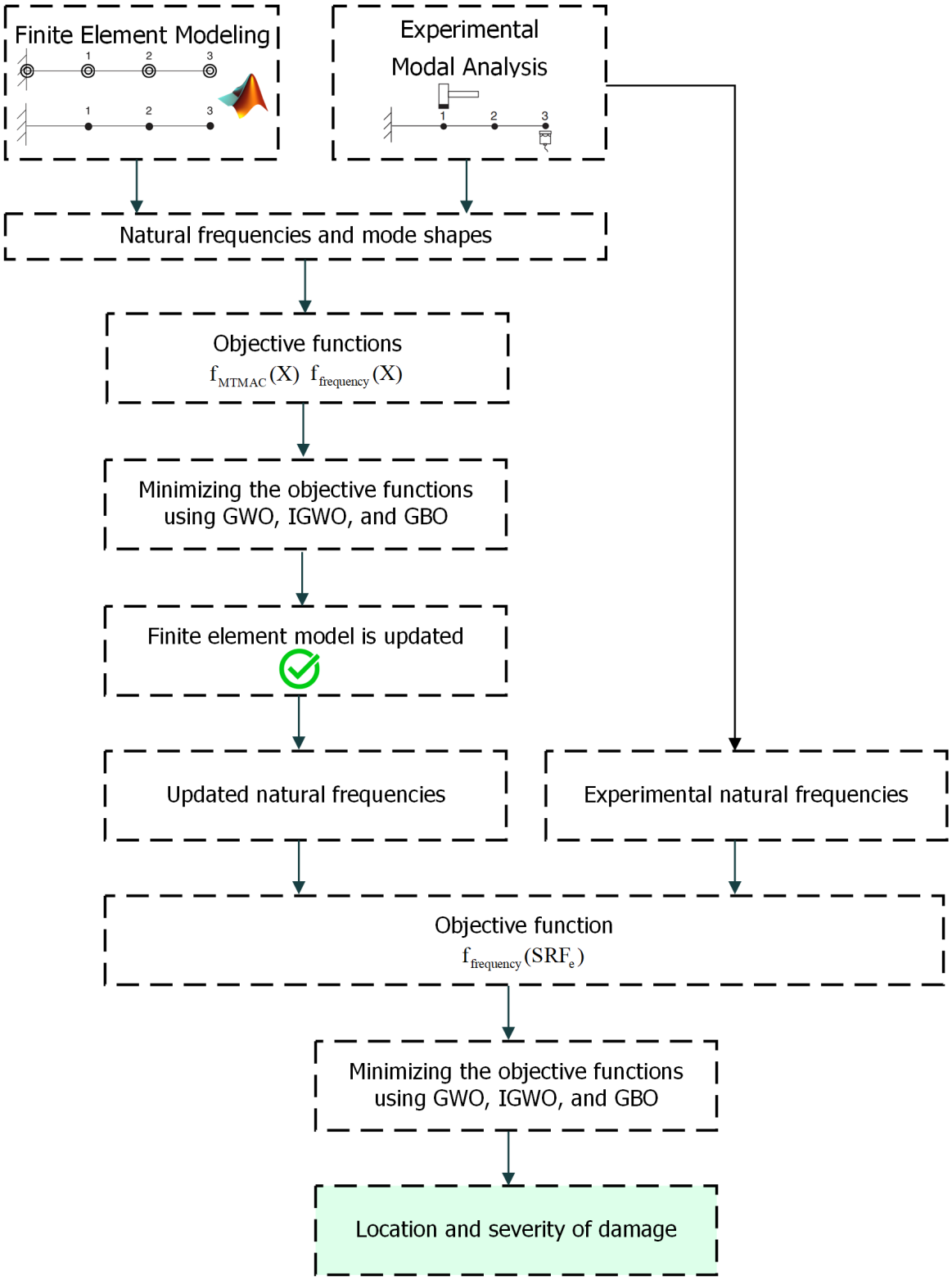

Figure 2. The flowchart of the damage identification strategy

3. Optimization algorithms

The aforementioned objective functions are minimized using three optimization algorithms: GWO, IGWO, and GBO. This section gives a brief explanation and mathematical description of each algorithm.

3.1. Grey wolf optimizer (GWO)

The social leadership and hunting tactics of grey wolves in nature served as inspiration for the grey wolf optimizer (GWO) algorithm. The GWO algorithm believes that three leader wolves, α, β, and δ, are the best solutions for leading the remaining wolves, ω wolves, in the direction of promising locations to discover the global solution. The three primary phases of wolf hunting are encircling, hunting, and attacking the target [60, 75].

Encircling phase: It is possible to simulate how the grey wolves encircle the prey, as shown in Eqs. (12) and (13).

$$\vec{D} = \left| \vec{C}.\vec{X}_p(t) - \vec{X}(t) \right| \tag{12}$$

$$\vec{X}(t+1) = \vec{X}_p(t) - \vec{A}.\vec{D} \tag{13}$$

where t represents the current iteration, $\vec{A}$ and $\vec{C}$ are coefficient vectors, $\vec{X}_p$ is the position vector of the prey, and $\vec{X}$ represents the position vector of a grey wolf. The vectors $\vec{A}$ and $\vec{C}$ are determined as follows:

$$\vec{A} = 2\vec{a}.\vec{r}_1 - \vec{a} \tag{14}$$

$$\vec{C} = 2.\vec{r}_2 \tag{15}$$

where a is linearly decreased from 2 to 0 over the course of iterations and $\vec{r}_1$, $\vec{r}_2$ are random vectors in [0, 1].

Hunting phase: It is supposed that α, β, and δ are more knowledgeable about the location of the prey. The other wolves (ω) are then required to follow the three best solutions, α, β, and δ, by taking into account their positions. The hunting behavior is given in the following equations:

$$\vec{D}_\alpha = \left| \vec{C}_1.\vec{X}_\alpha - \vec{X} \right|, \quad \vec{D}_\beta = \left| \vec{C}_2.\vec{X}_\beta - \vec{X} \right|, \quad \vec{D}_\delta = \left| \vec{C}_3.\vec{X}_\delta - \vec{X} \right| \tag{16}$$

$$\vec{X}_1 = \vec{X}_\alpha - \vec{A}_1.(\vec{D}_\alpha), \quad \vec{X}_2 = \vec{X}_\beta - \vec{A}_2.(\vec{D}_\beta), \quad \vec{X}_3 = \vec{X}_\delta - \vec{A}_3.(\vec{D}_\delta) \tag{17}$$

In Eq.(16), the first three best solutions at iteration t are denoted by X_α, X_β, and X_δ.

$$\vec{X}(t+1) = \frac{\vec{X}_1 + \vec{X}_2 + \vec{X}_3}{3} \tag{18}$$

Attacking phase: The hunt is over when the prey stops moving, and the wolves begin their attack. This procedure can be represented mathematically by using the value of $\vec{\alpha}$, which decreases linearly over the number of iterations, to manage exploration and exploitation.

3.2 Improved grey wolf optimizer (IGWO)

When using the GWO, α, β, and δ guide ω wolves to explore spaces that have the potential for discovering the best solution. However, trapping in the local optima may result from this behavior. Another shortcoming of the standard GWO is the reduction of the variety of the population, which makes the algorithm fall towards the local optimum. An improved grey wolf optimizer (IGWO) has been introduced by Nadimi-Shahraki et al. [60] to address the shortcomings of standard GWO. The initializing, movement, and selecting and updating are the three phase of the IGWO.

Initialization phase: N wolves are dispersed randomly by Eq. (19) in the search space between $[l_i, u_j]$.

$$X_{ij} = l_j + rand_j[0,1] \times (u_j - l_j), i \in [1, N], j \in [1, D] \tag{19}$$

Movement phase: Individual hunting is a remarkable social behavior of grey wolves in addition to group hunting, enabling us to improve the standard GWO. The dimension learning-based hunting (DLH) search technique is a further movement technique used by the IGWO. Each wolf in DLH is learned by its neighbors as a candidate for the new position. The new position of the wolf is determined as follows:

$$X_{i-DLH,d}(t+1) = X_{i,d}(t) + rand \times (X_{n,d}(t) - X_{r,d}(t)) \tag{20}$$

Selecting and updating phase: The superior candidate is initially determined in this phase by comparing the fitness values of the two candidates $X_{i-GWO}(t+1)$ and $X_{i-DLH}(t+1)$ according to Eq. (21). If the fitness value of the selected candidate is smaller than $X_i(t)$, $X_i(t)$ is updated by the selected candidate to update the new position of $X_i(t+1)$. $X_i(t)$ else stays the same.

$$X(t+1) = \begin{cases} X_{i-GWO}(t+1), & if\ f(X_{i-GWO}) < f(X_{i-DLH}) \\ X_{i-DLH}(t+1) & otherwise \end{cases} \tag{21}$$

where $X_{i-GWO}(t+1)$ is calculated by Eq. (18).

3.3. Gradient-based optimizer (GBO)

Ahmadianfar et al. [76] proposed gradient-based optimization (GBO) that incorporates gradient and population-based methods. The GBO relies on two operators, each of whom has a specific responsibility, to update the solutions. The gradient search rule (GSR) is the first operator, and it is used to enhance exploration. The second operator, known as a local escaping operator (LEO), is utilized to improve the capacity for exploitation [77].

A population X with N solutions is created as the first step in GBO using the following formulae:

$$x_i = x_{\min} + rand \times (x_{\max} - x_{\min}), \quad i = 1,2,...,N \tag{22}$$

where x_{min} and x_{max} are the bounds of the search space and *rand* represent a random number between 0 and 1. Then, the best solution is selected after computing the fitness value for each.

The solutions $\left(x_i^{It}, i = 1,2,...,N\right)$ in the direction $\left(x_b - x_i^{It}\right)$ are then updated using the GSR and direction movement. To perform this updating procedure, the new three solutions $x1_i^{It}$, $x2_i^{It}$, and $x3_i^{It}$ are computed in the manner described below:

$$x1_i^{It} = x_i^{It} - GSR + rand \times \rho_1 \times \left(x_b - x_i^{It}\right) \tag{23}$$

where x_b represents the best solution and ρ_1 is operated in the optimization process to achieve a more reasonable balance of exploration and exploitation, and can be defined as follows:

$$\rho_1 = 2 \times rand \times \alpha - \alpha \tag{24}$$

Where:

$$\alpha = \left|\beta \times \sin\left(3\pi/2 + \sin\left(\beta \times 3\pi/2\right)\right)\right| \tag{25}$$

$$\beta = \beta_{\min} + \left(\beta_{\max} - \beta_{\min}\right) \times \left(1 - \left(It / Max_{It}\right)^3\right)^2 \tag{26}$$

where β_{min} and β_{max} are defined as 0.2 and 1.2, respectively. *It* represents the current iteration, and Max_{It} shows the total number of iterations.

The following equation defines the GSR:

$$GSR = randn \times \rho_2 \times \left(2 \times \Delta x \times x_i^{It}\right) / \left(yp_i - yq_i + \varepsilon\right) \tag{27}$$

where ε is a small value between [0, 0.1] and *randn* is a random number with a normal distribution. ρ_2 is obtained according to Eq. (24). Δx and δ can be respectively defined as:

$$\Delta x = rand\left(1:N\right) \times \left|\left(\left(x_b - x_{r1}^{It}\right) + \delta\right) / 2\right| \tag{28}$$

$$\delta = 2 \times rand \times \left(\left|\left(x_{r1}^{It} + x_{r2}^{It} + x_{r3}^{It} + x_{r4}^{It}\right) / 4 - x_i^{It}\right|\right) \tag{29}$$

where *rand(1 : N)* is a N-dimensional random vector, r_1, r_2, r_3, and r_4 are radomly selected integers between [1, *N*].

Eqs. (30) and (31) are applied to update the locations yp_i and yq_i :

$$yp_i = rand \times \left(x_s + x_i\right) / 2 + rand \times \Delta x \tag{30}$$

$$yq_i = rand \times \left(x_s + x_i\right) / 2 - rand \times \Delta x \tag{31}$$

where:

$$x_s = x_i - randn \times \left(2 \times \Delta x \times x_i\right) / \left(x_{worst} - x_b + \varepsilon\right) \tag{32}$$

A new solution at iteration $It + 1$ is produced based on the positions $x1_i^{It}$, $x2_i^{It}$, and $x3_i^{It}$:

$$x_i^{It+1} = r_a \times \left(r_b \times x1_i^{It} + \left(1 - r_b\right) \times x2_i^{It}\right) + \left(1 - r_a\right) \times x3_i^{It} \tag{33}$$

where r_a and r_b are two randomly generated integers. The following definitions of $x2_i^{It}$ and $x3_i^{It}$ are possible:

$$x2_i^{It} = x_b - GSR + rand \times \rho_2 \times \left(x_{r1}^{It} - x_{r2}^{It}\right) \tag{34}$$

$$x3_i^{It} = x_i^{It} - \rho_1 \times \left(x2_i^{It} - x1_i^{It}\right) \tag{35}$$

The LEO is used to increase the GBO's capacity for exploitation. This is accomplished by updating the solution x_i^{It} using the following equation in accordance with the probability *pr*:

$$x_i^{It+1} = \begin{cases} x_i^{It} + f_1 \times W_1 + f_2 \times \rho_1 \times W_3 + u_2 \times W_2 / 2 & pr < 0.5 \\ x_b + f_1 \times W_1 + f_2 \times \rho_1 \times W_3 + u_2 \times W_2 / 2 & otherwise \end{cases} \tag{36}$$

where:

$$W_1 = \left(u_1 \times x_b - u_2 \times x_k^{It}\right) \tag{37}$$

$$W_2 = \left(x_{r1}^{It} - x_{r2}^{It}\right) \tag{38}$$

$$W_3 = \left(u_3 \times \left(x\,2_i^{It} - x\,1_i^{It}\right)\right) \tag{39}$$

In Eq. (36) to (39), f_1, f_2, u_1, u_2, and u_3 are random integers, and x_k^{It} is also calculated by the proposed scheme in Ref. [76].

4. Experimental example

An experimental steel beam with a free-free boundary condition is used to verify the effectiveness of the proposed method for FEM updating and damage identification, as shown in Figure 3. The material properties, including Young's modulus, mass density, and Poisson's ratio, are listed in Table 1. The dimensions of the laboratory-scale beam are also given in Table 2.

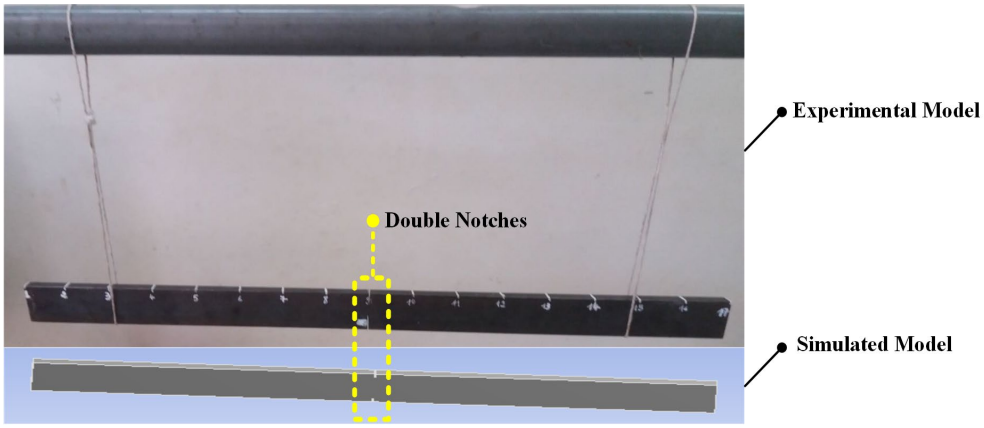

Figure 3. Experimental set-up and simulated model of the free-free beam

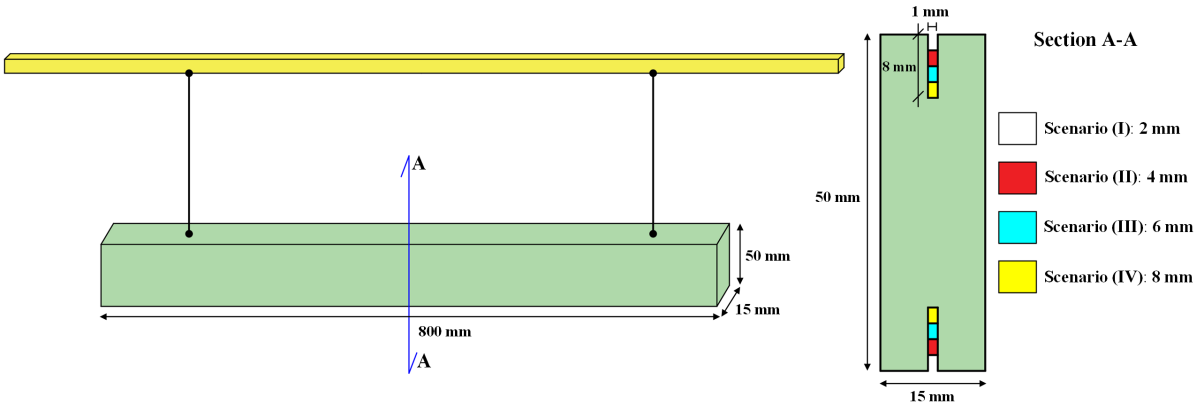

Figure 4. Dimension of the free-free beam with different crack scenarios (not to scale)

Table 1. The material properties of the experimental beam

Young's modulus (N/mm^2)	Mass density (kg/m^3)	Poisson's ratio
2.18×10^{11}	7800	0.3

Table 2. The dimensions of the experimental beam

Length (m)	Height (m)	Width (m)
0.8	0.05	0.015

The impact hammer (PCB 086C03) is utilized to excite the free-free beam by the induced force and measure the acceleration responses using accelerometers (356A15) to perform experimental modal analysis. The data acquisition system (NI cDAQ-9184) and signal analyzer software (m+p SO Analyzer 4.3) are employed to collect and interpret the acceleration responses, respectively. The experimental facilities to conduct the modal analysis are shown in Figure 5.

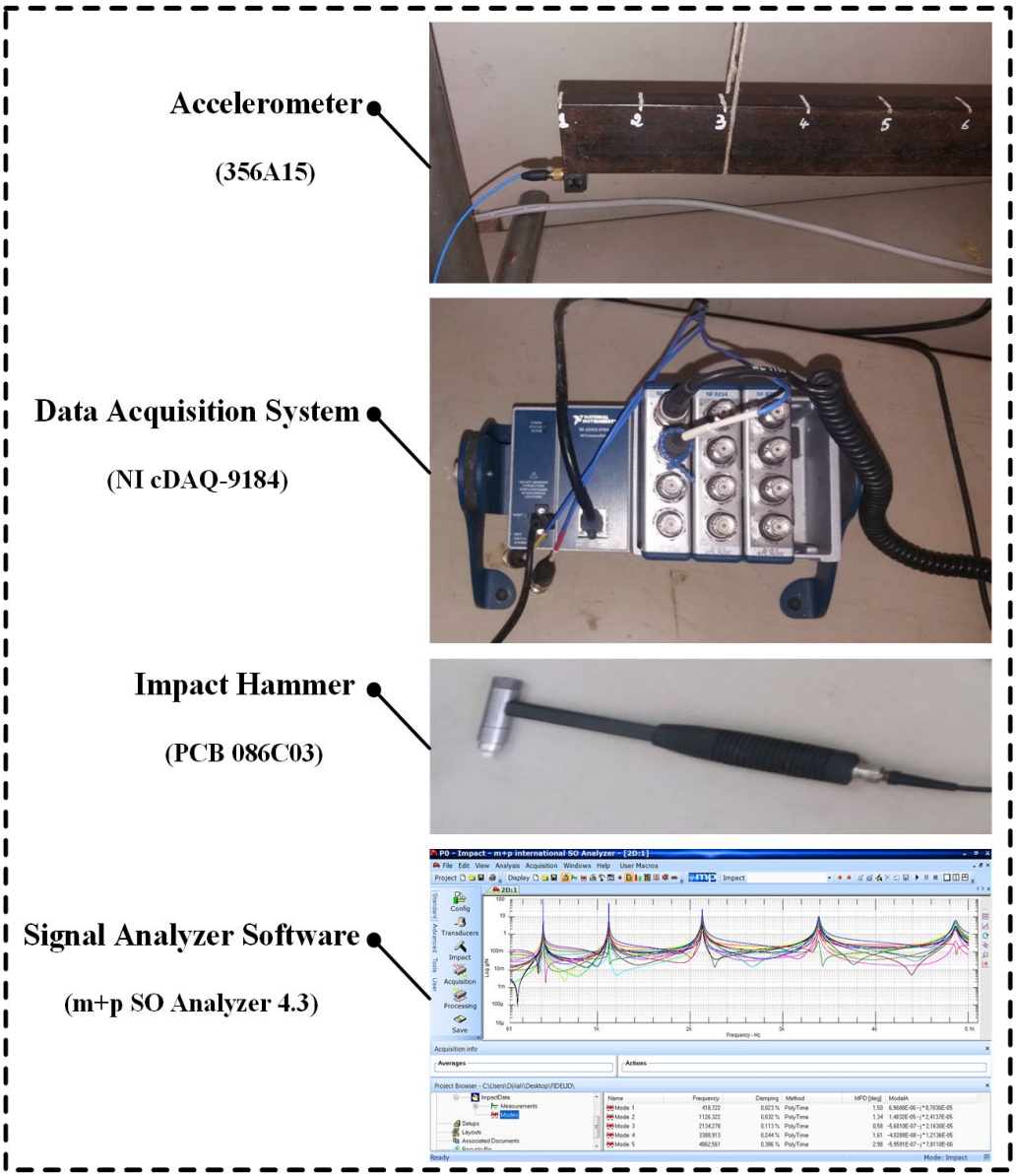

Figure 5. The experimental facilities for modal analysis

The peak picking method is also implemented to estimate the modal properties of the acquired signals. Figure 6 and Figure 7 illustrate the force-time history and acceleration-time history of the intact beam, respectively.

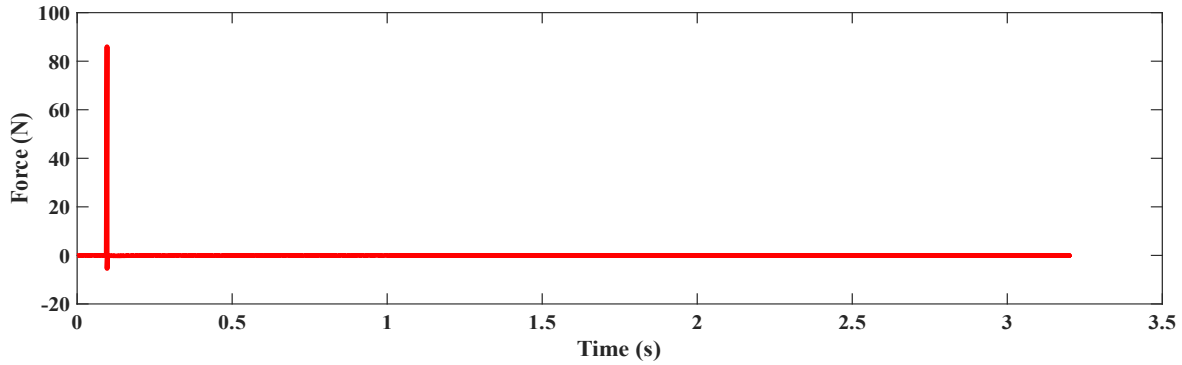

Figure 6. The force-time history of the intact beam

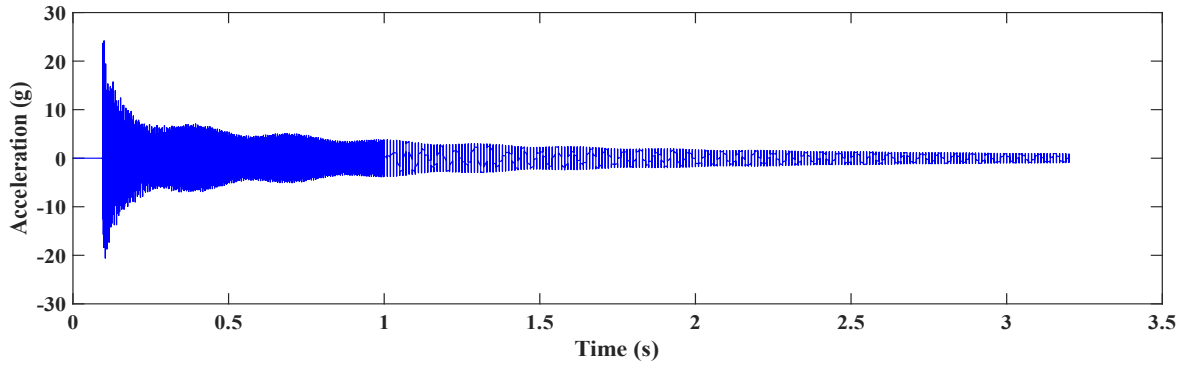

Figure 7. The acceleration-time history of the intact beam

The frequency response function (FRF) of the intact beam is depicted in Figure 8, and the experimental mode shapes are presented in Figure 9.

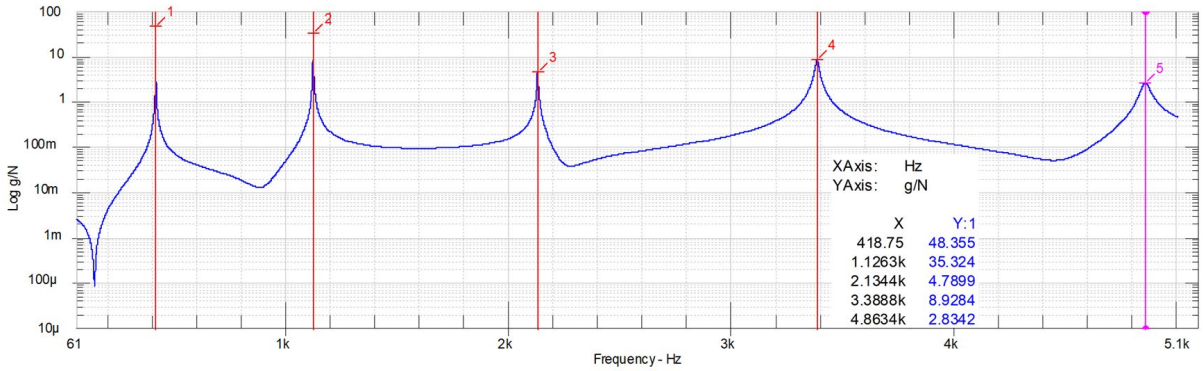

Figure 8. The experimental FRF of the intact free-free beam

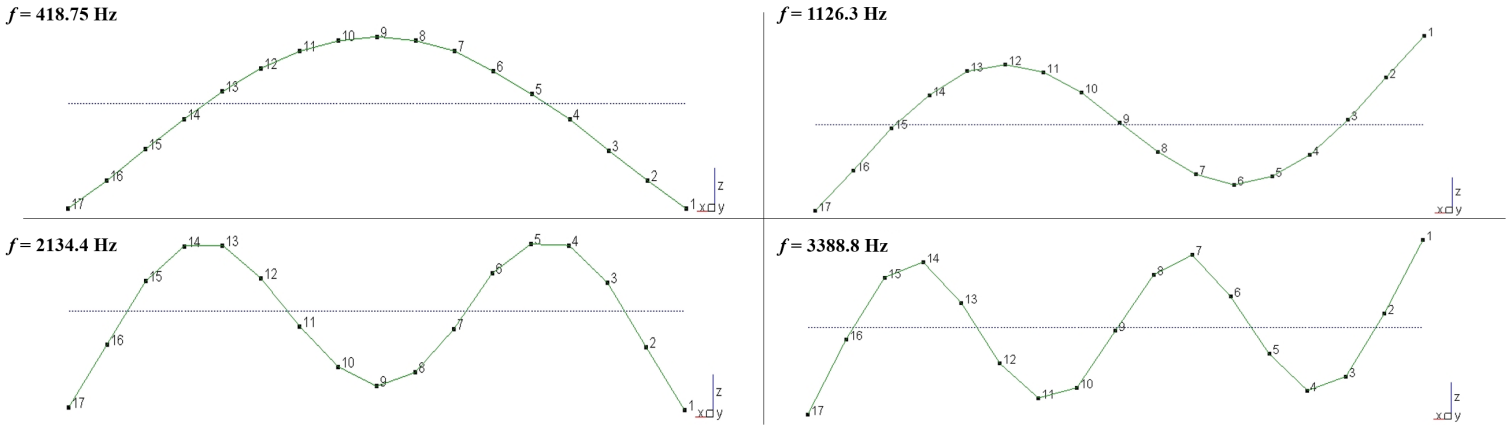

Figure 9. The experimental mode shapes of the intact free-free beam

The following four crack scenarios (double notches), according to Figure 4, were embedded in the middle of the free-free beam:

Scenario (I): 2 mm

Scenario (II): 4 mm

Scenario (III): 6 mm

Scenario (IV): 8 mm

Figures 10 to 13 show the FRFs and extracted natural frequencies of four crack scenarios. It is clearly indicated that the natural frequencies decreased after introducing crack scenarios.

The experimental modal analysis was repeated 17 times for healthy and four crack scenarios to examine the variability in measured data. Figure 14 displays the standard deviations and mean natural frequencies of 17 individual trials. In the undamaged condition and all cracked models, the standard deviations for the 5th mode are more extensive than the first four modes. To avoid false identification in damage detection methodology and develop an accurate model updating approach, this study adopts the first four natural frequencies because of the relatively small variation in 17 times measurements. The standard deviations in the undamaged dataset are considerably smaller than those calculated in crack scenarios. In damaged conditions, variations in different trials, especially in higher modes, are generally expected and can be observed in most measurements. For instance, the presented database by Esu [78] for pipeline monitoring is available for more studies.

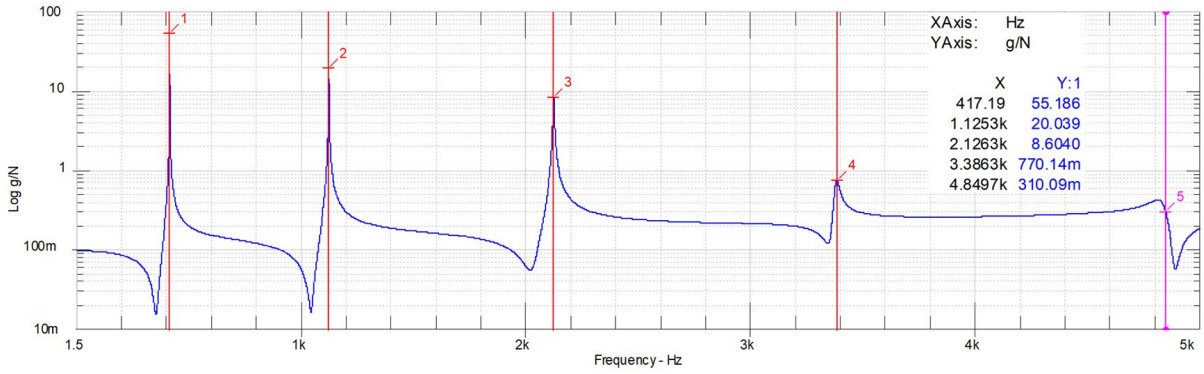

Figure 10. The experimental FRF of the cracked free-free beam - double notches (2 mm)

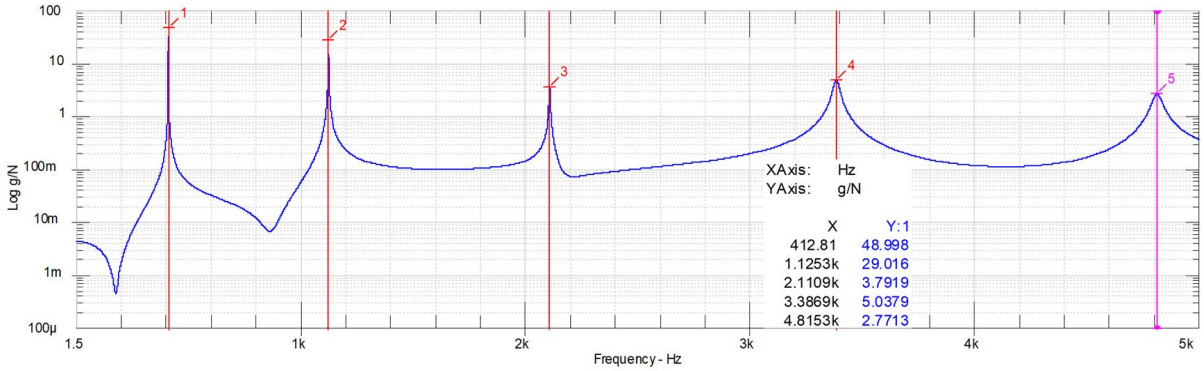

Figure 11. The experimental FRF of the cracked free-free beam - double notches (4 mm)

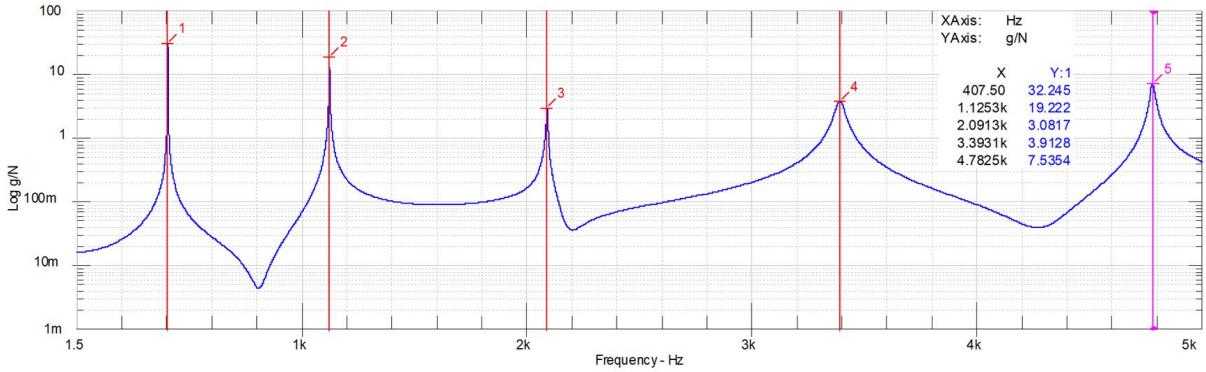

Figure 12. The experimental FRF of the cracked free-free beam - double notches (6 mm)

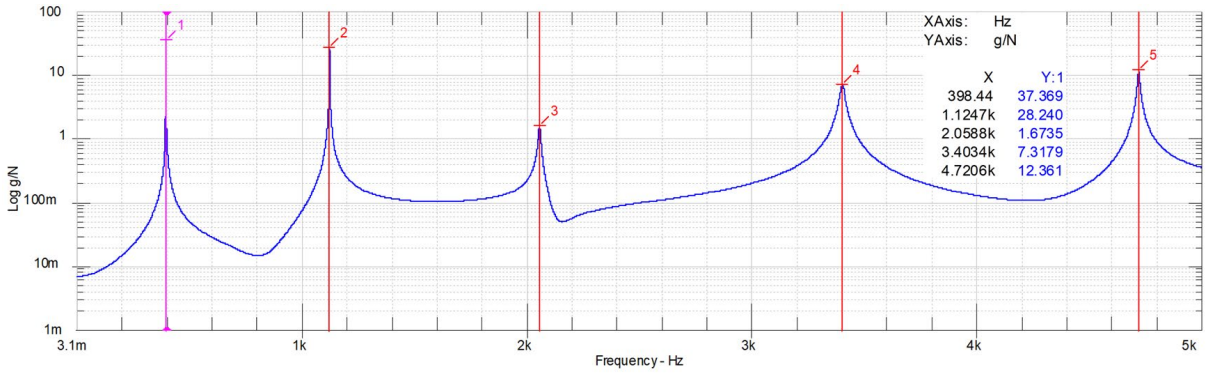

Figure 13. The experimental FRF of the cracked free-free beam - double notches (8 mm)

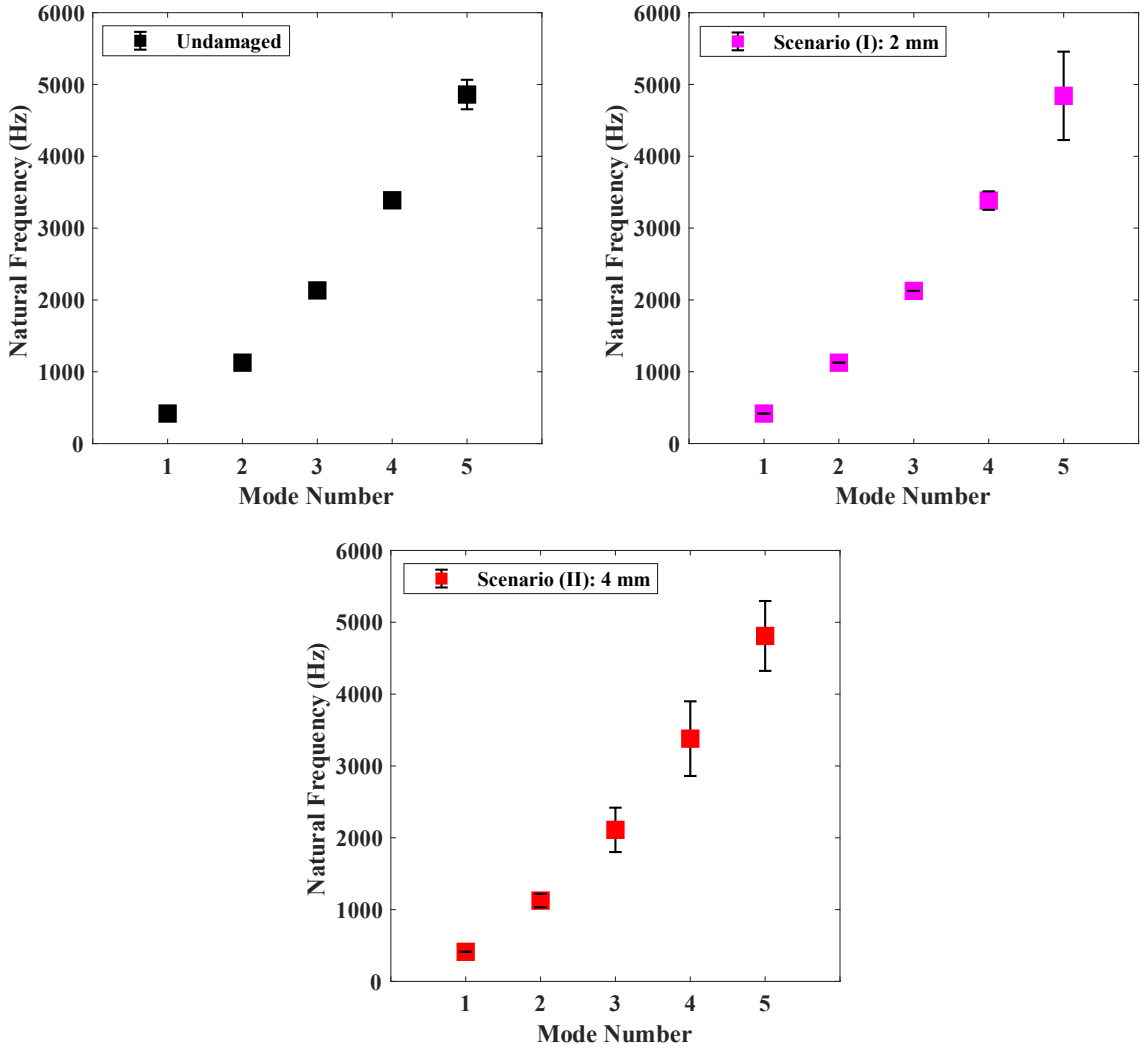

Figure 14. The standard deviations and mean natural frequencies of different measurements (error bars were multiplied by 100 and exaggeratedly plotted)

5. Results and discussion

Ten individual runs are performed for each FEM updating state and crack scenario to provide statistical results, computing time, and convergence curves. All computations were carried out using the MATLAB programming and computing platform on a laptop with an Intel (R) Core (TM) i7-6700 HQ, 8 GB RAM, and a 2.60 GHz CPU. During the optimization-based model updating procedure, ±50% of Young's modulus and the end fixity factor of all elements are considered as the bounds of search space. Additionally, the upper bound and lower bound of exploration in the damage detection step are 1 and -1, respectively.

Table 3 presents the statistical results of FEM updating obtained by the semi-rigidly connected frame element when applying different optimization algorithms (GWO, IGW, and GBO) and two objective functions based on MTMAC and changes in the natural frequencies. The worst value for each state is in bold. As shown in Table 3, the performance of GWO-MTMAC and

IGWO-MTMAC is the most reasonable. The updated first four natural frequencies and the corresponding mode shapes (MAC) of the free-free beam have a complete agreement with the measured modal data. In contrast, several errors are observed in the fourth mode when using the GBO-MTMAC. The statistical results of FEM updating based on the GWO-Frequency, IGWO-Frequency, and GBO-Frequency demonstrates acceptable accuracy for natural frequencies. However, there are some difficulties in establishing a good correlation between experimental and updated mode shapes. Therefore, using the changes in natural frequencies as an objective function could not provide the best results when applying different optimization algorithms (GWO, IGWO, and GBO). The statistical results of FEM updating based on the Euler-Bernoulli beam element are presented in Table 4. When using IGWO–MTMAC, GWO-MTMAC, and GBO-MTMAC for FEM calibration, the correlation between updated and experimental mode shapes are almost acceptable. However, these algorithms and the objective function based on MTMAC could not provide significant results in updating frequencies, and relatively large errors are observed for all modes. As illustrated in Table 4, It is found that the GWO-Frequency, IGWO–Frequency, and GBO-Frequency fail to update the numerical model, and there is a poor agreement between experimental and updated models. Overall, the obtained results for FEM updating of the free-free beam based on the semi-rigidly connected frame element and employing GWO-MTMAC and IGWO-MTMAC are more efficient than those obtained from the same algorithms and objective function when utilizing the Euler-Bernoulli beam element.

Figure 15 shows the convergence curves of the objective function values relying on GWO, GBO, and IGWO. It is clearly observed that the convergence of IGWO and GBO is better than GWO, which means these algorithms can provide more satisfactory results for identifying the 2 mm crack. In addition, the convergence speed of the GBO is much faster than IGWO. The IGWO needs more iterations to converge (approximately 500). However, the GBO takes only less than 40 iterations. The statistical results of damage detection (double notches-2 mm) based on the GWO, GBO, and IGWO are demonstrated in Table 5 and Figure 16. The GBO and IGWO produce the best competitive results with the best mean value of the damage severity and minor standard deviation. GWO could find the damaged element with adequate accuracy. However, some false identifications with considerable standard deviation exist, especially at the 16^{th} element. Therefore, the statistical results for the 2 mm crack identification illustrate the robustness of the GBO and IGWO. As shown in Figure 17, the IGWO needs significant computational effort to find the optimal solution. In contrast, the GWO and GBO only need

about 7 minutes.

The convergence curves of the cost function values during the optimization procedure to determine the location and severity of the 4 mm crack based on GWO, GBO, and IGWO are displayed in Figure 18. Similar to the previous damage scenario (2 mm crack), GBO converges much faster than GWO and IGWO. Besides, the GBO and IGWO are pretty closer to the global optimum. Therefore, accurate results of damage identification are expected when applying the GBO and IGWO. Table 6 and Figure 19 present the statistical results of damage detection in the second scenario (4 mm crack). At first glance, the obtained results by all optimization algorithms seem excellent. The GWO is capable of identifying the location and severity of the damage. However, small false alarms exist at the 4^{th} and 5^{th} elements with minor standard deviations. It should be mentioned that when using the GBO and IGWO, only one false identification is observed at the 5^{th} element. Generally, all algorithms yield the accurate mean value of the damage severity. The computation time to solve the optimization problem of crack identification (4 mm crack) based on IGWO is much greater than other algorithms, as shown in Figure 20. Similar to the previous damage scenario (2 mm crack), the GWO and GBO have the nearly same computation time.

Figure 21 displays the convergence curves of the objective function values for solving the inverse problem of the crack identification (6 mm crack) based on GWO, GBO, and IGWO. It is clear that the convergence rate of the IGWO is considerably improved compared to GWO. Besides, the lowest convergence rate is related to GBO, which may appear in poor crack detection results. The statistical results of crack identification (double notches-6 mm) based on the GWO, GBO, and IGWO are listed in Table 7. For visualization of statistical results, the mean value with plus and minus standard deviation are plotted in Figure 22. The IGWO could locate the damaged element without false alarms on healthy members. However, the other two algorithms (GWO and GBO) could not find the promising stiffness reduction factor for the 8^{th} element, and there are also two false identifications (5^{th} and 9^{th} elements). The computation time of IGWO is more expensive than two other algorithms, as shown in Figure 23. The considerable computation time is not a drawback for IGWO because the IGWO is more efficient in dealing with the crack identification problem.

The convergence curves of the cost function values of the last crack identification scenario (8 mm crack) are presented in Figure 24. It can be found that the IGWO algorithm can converge to the optimal solution more effectively than the two other algorithms. Similar to the previous

scenario (6 mm crack), the most powerless convergence rate referred to the GBO algorithm. The poor convergence rate of GBO has resulted in unsatisfactory crack identification results, as statistically demonstrated in Table 8 and Figure 25. For further investigation, when using GBO, the mean stiffness reduction of false alarms at the 5^{th} and 9^{th} elements is more considerable than the false identification by the GWO. In contrast, the IGWO can successfully determine the exact damaged element and its severity without any false identification. Regarding the computational cost, the IGWO algorithm requires about 15 minutes (see Figure 26), which is the highest computation time among the two other algorithms.

Table 9 summarizes the performance of objective functions and optimization algorithms when considering the Euler-Bernoulli beam element and S-RCFE for FEM updating. A tick mark is used to indicate which ones are the best.The performance of optimization algorithms for crack identification in different scenarios is also embedded in Table 10.

Table 3. Statistical results of FEM updating with the semi-rigidly connected frame element

Mode		1	2	3	4
Experimental f (Hz)		418.7500	1126.3000	2134.4000	3388.8000
GWO-MTMAC	mean f (Hz)	418.7508	1126.2937	2134.3861	3388.8207
	std f	1.5495E-03	7.9767E-03	1.1733E-02	2.8842E-02
	error f (%)	1.9450E-04	5.5550E-04	6.5042E-04	6.1042E-04
	mean MAC	0.9992	0.9970	0.9962	0.9956
	std MAC	2.7396E-04	6.3988E-04	3.5617E-04	2.5946E-04
IGWO-MTMAC	mean f (Hz)	418.7503	1126.2957	2134.3947	3388.7991
	std f	2.9998E-03	1.3867E-02	1.4436E-02	1.7047E-02
	error f (%)	7.4742E-05	3.8090E-04	2.5026E-04	2.5988E-05
	mean MAC	0.9991	0.9964	0.9970	0.9961
	std MAC	2.2109E-04	2.9503E-04	2.8524E-04	3.8151E-04
GBO-MTMAC	mean f (Hz)	418.7497	1126.2981	2134.3903	3431.5377
	std f	1.8549E-03	3.1523E-03	3.7359E-02	**3.8709E+01**
	error f (%)	6.5732E-05	1.6708E-04	4.5485E-04	**1.2454E+00**
	mean MAC	0.9989	0.9979	0.9955	**0.9936**
	std MAC	5.6443E-04	8.8633E-04	6.7137E-04	1.7536E-03
GWO-Frequency	mean f (Hz)	418.7500	1126.3046	2134.3933	3388.7927
	std f	4.1633E-03	1.4120E-02	1.8393E-02	3.7391E-02
	error f (%)	4.7311E-06	4.1042E-04	3.1468E-04	2.1574E-04
	mean MAC	**0.3959**	**0.8156**	**0.9588**	**0.9829**
	std MAC	1.9452E-01	1.0493E-01	2.4970E-02	9.9230E-03
IGWO-Frequency	mean f (Hz)	418.7532	1126.2989	2134.4133	3388.7950
	std f	5.8050E-03	1.0154E-02	1.7883E-02	3.4668E-02
	error f (%)	7.6481E-04	9.8779E-05	6.2212E-04	1.4623E-04
	mean MAC	**0.4107**	**0.7898**	**0.9505**	**0.9879**
	std MAC	1.0202E-01	4.6908E-02	1.9522E-02	6.2672E-03
GBO-Frequency	mean f (Hz)	418.7500	1126.3000	2134.4000	3388.8000
	std f	9.4414E-12	2.5420E-11	3.5756E-11	7.5206E-11
	error f (%)	1.0045E-12	5.6525E-13	8.0961E-13	5.0993E-13
	mean MAC	**0.7684**	**0.9691**	**0.9874**	**0.9914**
	std MAC	1.5845E-01	3.1417E-02	5.0029E-03	3.9214E-03

Table 4. Statistical results of FEM updating with Euler-Bernoulli beam element

Mode		1	2	3	4
Experimental f (Hz)		418.7500	1126.3000	2134.4000	3388.8000
GWO-MTMAC	mean f (Hz)	410.6928	1113.1081	2134.4000	3497.0376
	std f	7.4457E-03	2.0813E-02	2.5369E-04	9.1939E-02
	error f (%)	**1.9619E+00**	**1.1851E+00**	1.4463E-06	**3.0951E+00**
	mean MAC	0.9993	0.9989	0.9950	**0.9924**
	std MAC	1.7625E-07	1.0590E-06	5.0950E-06	1.0910E-05
IGWO-MTMAC	mean f (Hz)	410.7103	1113.1230	2134.3997	3497.0941
	std f	1.1885E-03	1.7761E-03	2.0935E-03	1.2615E-02
	error f (%)	**1.9575E+00**	**1.1838E+00**	1.3847E-05	**3.0967E+00**
	mean MAC	0.9993	0.9989	0.9950	**0.9924**
	std MAC	1.5383E-07	1.1489E-06	6.1676E-07	2.1913E-06
GBO-MTMAC	mean f (Hz)	410.7133	1113.1256	2134.4000	3497.1074
	std f	3.8863E-07	3.1530E-07	2.5406E-08	1.6249E-05
	error f (%)	**1.9568E+00**	**1.1836E+00**	5.3854E-10	**3.0971E+00**
	mean MAC	0.9993	0.9989	0.9950	**0.9924**
	std MAC	1.9661E-09	1.5125E-08	4.4580E-09	1.5441E-08
GWO-Frequency	mean f (Hz)	411.8114	1122.8082	2140.7551	3386.6501
	std f	2.4541E-02	2.4294E-01	1.0952E-01	1.9630E-01
	error f (%)	**1.6849E+00**	**3.1099E-01**	**2.9686E-01**	**6.3481E-02**
	mean MAC	0.9992	0.9960	**0.9630**	**0.8741**
	std MAC	4.1325E-05	8.6039E-04	7.9171E-03	2.4509E-02
IGWO-Frequency	mean f (Hz)	411.8355	1122.9640	2140.6599	3386.5661
	std f	6.1212E-04	8.3138E-03	3.0374E-02	8.7090E-02
	error f (%)	**1.6789E+00**	**2.9707E-01**	**2.9243E-01**	**6.5964E-02**
	mean MAC	0.9992	0.9954	**0.9581**	**0.8616**
	std MAC	4.0825E-05	4.0464E-04	1.7477E-03	7.3734E-04
GBO-Frequency	mean f (Hz)	411.8142	1122.7285	2140.7414	3386.7589
	std f	2.7523E-02	3.0316E-01	1.1287E-01	2.6424E-01
	error f (%)	**1.6842E+00**	**3.1811E-01**	**2.9623E-01**	**6.0266E-02**
	mean MAC	0.9992	0.9962	**0.9662**	**0.8852**
	std MAC	4.0131E-05	1.0936E-03	1.0089E-02	3.0645E-02

Table 5. The statistical results of damage detection-Scenario (I): 2 mm

Element	SRF (GWO)		SRF (GBO)		SRF (IGWO)	
	Mean	Std	Mean	Std	Mean	Std
1	0.0000	0.0000	0.0000	0.0000	0.0000	0.0000
2	0.0000	0.0000	0.0000	0.0000	0.0000	0.0000
3	0.0000	0.0000	0.0000	0.0000	0.0000	0.0000
4	**0.0119**	**0.0063**	**0.0148**	0.0000	**0.0148**	0.0000
5	**0.0016**	**0.0041**	0.0000	0.0000	0.0000	0.0000
6	0.0000	0.0000	0.0000	0.0000	0.0000	0.0000
7	0.0000	0.0000	0.0000	0.0000	0.0000	0.0000
8	0.0475	**0.0168**	0.0521	0.0000	0.0521	0.0000
9	**0.0046**	**0.0144**	0.0000	0.0000	0.0000	0.0000
10	0.0000	0.0000	0.0000	0.0000	0.0000	0.0000
11	0.0000	0.0000	0.0000	0.0000	0.0000	0.0000
12	0.0000	0.0000	0.0000	0.0000	0.0000	0.0000
13	**0.0012**	**0.0039**	0.0000	0.0000	0.0000	0.0000
14	0.0000	0.0000	0.0000	0.0000	0.0000	0.0000
15	0.0000	0.0000	0.0000	0.0000	0.0000	0.0000
16	**0.0228**	**0.0575**	0.0000	0.0000	0.0000	0.0000

Table 6. The statistical results of damage detection-Scenario (II): 4 mm

Element	SRF (GWO)		SRF (GBO)		SRF (IGWO)	
	Mean	Std	Mean	Std	Mean	Std
1	0.0000	0.0000	0.0000	0.0000	0.0000	0.0000
2	0.0000	0.0000	0.0000	0.0000	0.0000	0.0000
3	0.0000	0.0000	0.0000	0.0000	0.0000	0.0000
4	**0.0003**	**0.0004**	0.0000	0.0000	0.0000	0.0000
5	**0.0007**	**0.0008**	**0.0015**	0.0000	**0.0015**	0.0000
6	0.0000	0.0000	0.0000	0.0000	0.0000	0.0000
7	0.0000	0.0000	0.0000	0.0000	0.0000	0.0000
8	0.1849	**0.0001**	0.1848	0.0000	0.1848	0.0000
9	0.0000	0.0000	0.0000	0.0000	0.0000	0.0000
10	0.0000	0.0000	0.0000	0.0000	0.0000	0.0000
11	0.0000	0.0000	0.0000	0.0000	0.0000	0.0000
12	0.0000	0.0000	0.0000	0.0000	0.0000	0.0000
13	0.0000	0.0000	0.0000	0.0000	0.0000	0.0000
14	0.0000	0.0000	0.0000	0.0000	0.0000	0.0000
15	0.0000	0.0000	0.0000	0.0000	0.0000	0.0000
16	0.0000	0.0000	0.0000	0.0000	0.0000	0.0000

Table 7. The statistical results of damage detection-Scenario (III): 6 mm

Element	SRF (GWO)		SRF (GBO)		SRF (IGWO)	
	Mean	Std	Mean	Std	Mean	Std
1	0.0000	0.0000	0.0000	0.0000	0.0000	0.0000
2	0.0000	0.0000	0.0000	0.0000	0.0000	0.0000
3	0.0000	0.0000	0.0000	0.0000	0.0000	0.0000
4	0.0000	0.0000	0.0000	0.0000	0.0000	0.0000
5	**0.0013**	**0.0040**	**0.0038**	**0.0061**	0.0000	0.0000
6	0.0000	0.0000	0.0000	0.0000	0.0000	0.0000
7	0.0000	0.0000	0.0000	0.0000	0.0000	0.0000
8	0.2713	**0.0953**	0.2110	**0.1456**	0.3015	0.0000
9	**0.0280**	**0.0887**	**0.0841**	**0.1355**	0.0000	0.0000
10	0.0000	0.0000	0.0000	0.0000	0.0000	0.0000
11	0.0000	0.0000	0.0000	0.0000	0.0000	0.0000
12	0.0000	0.0000	0.0000	0.0000	0.0000	0.0000
13	0.0000	0.0000	0.0000	0.0000	0.0000	0.0000
14	0.0000	0.0000	0.0000	0.0000	0.0000	0.0000
15	0.0000	0.0000	0.0000	0.0000	0.0000	0.0000
16	0.0000	0.0000	0.0000	0.0000	0.0000	0.0000

Table 8. The statistical results of damage detection-Scenario (IV): 8 mm

Element	SRF (GWO)		SRF (GBO)		SRF (IGWO)	
	Mean	Std	Mean	Std	Mean	Std
1	0.0000	0.0000	0.0000	0.0000	0.0000	0.0000
2	0.0000	0.0000	0.0000	0.0000	0.0000	0.0000
3	0.0000	0.0000	0.0000	0.0000	0.0000	0.0000
4	0.0000	0.0000	0.0000	0.0000	0.0000	0.0000
5	**0.0018**	**0.0056**	**0.0107**	**0.0092**	0.0000	0.0000
6	0.0000	0.0000	0.0000	0.0000	0.0000	0.0000
7	0.0000	0.0000	0.0000	0.0000	0.0000	0.0000
8	0.3558	**0.1875**	0.1779	**0.2297**	0.4447	0.0000
9	**0.0851**	**0.1794**	**0.2544**	**0.2190**	0.0000	0.0000
10	0.0000	0.0000	0.0000	0.0000	0.0000	0.0000
11	0.0000	0.0000	0.0000	0.0000	0.0000	0.0000
12	**0.0001**	**0.0002**	0.0000	0.0000	0.0000	0.0000
13	0.0000	0.0000	0.0000	0.0000	0.0000	0.0000
14	0.0000	0.0000	0.0000	0.0000	0.0000	0.0000
15	0.0000	0.0000	0.0000	0.0000	0.0000	0.0000
16	0.0000	0.0000	0.0000	0.0000	0.0000	0.0000

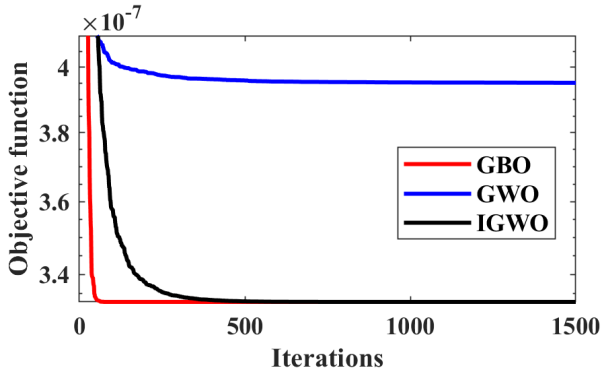

Figure 15. The convergence curves of the objective function values-Scenario (I): 2 mm

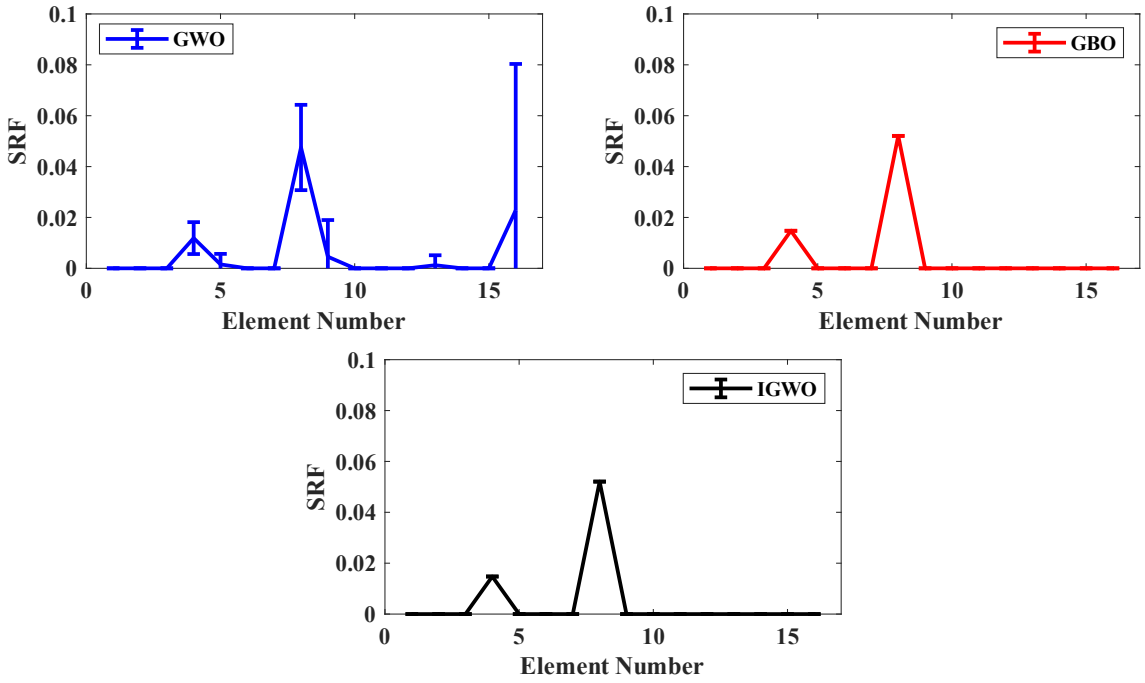

Figure 16. Identified results by using GWO, GBO, and IGWO-Scenario (I): 2 mm

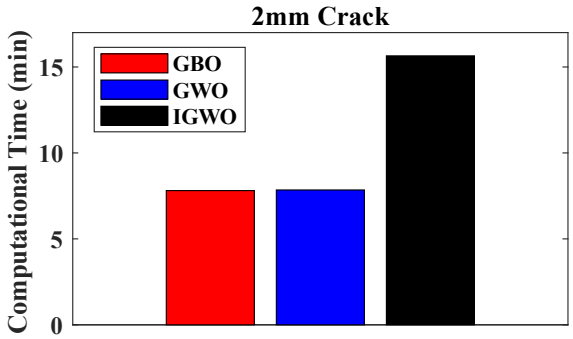

Figure 17. The computation time of 2 mm crack identification based on GWO, GBO, and IGWO-Scenario (I)

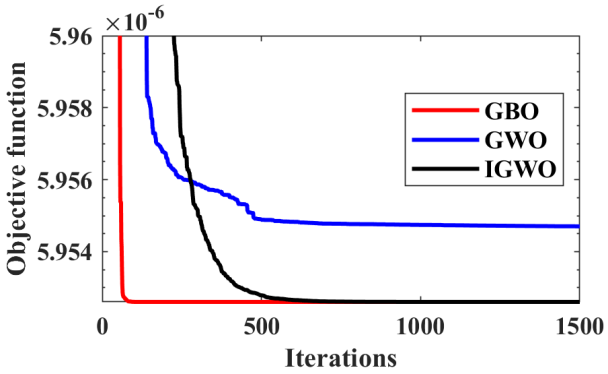

Figure 18. The convergence curves of the objective function values-Scenario (II): 4 mm

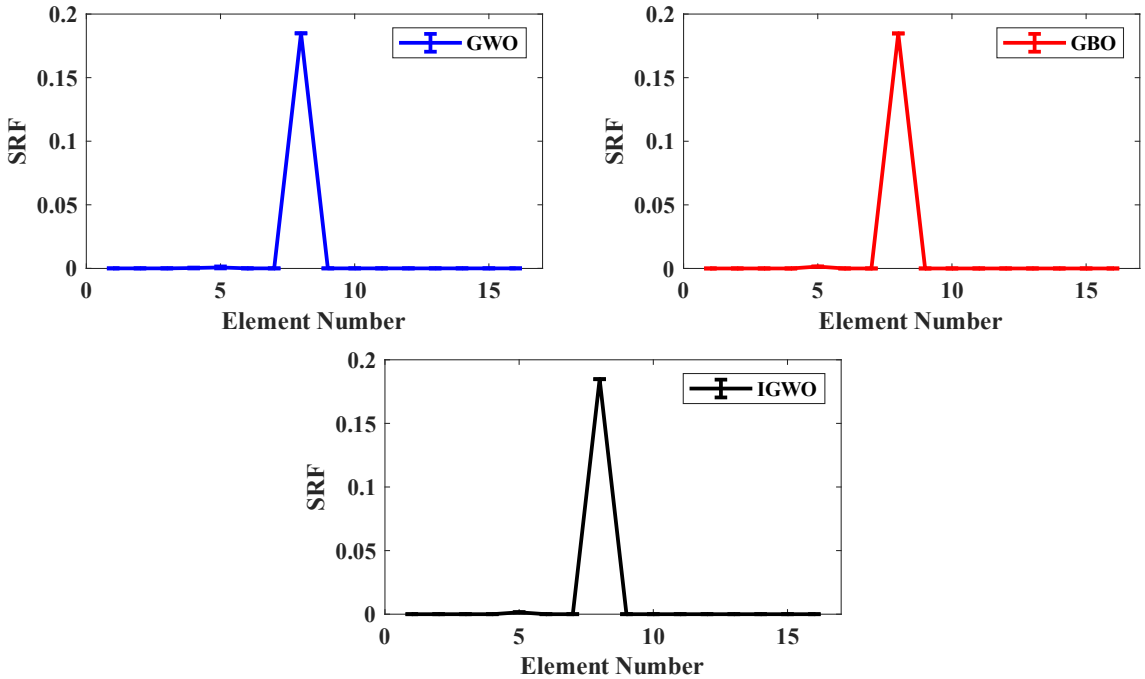

Figure 19. Identified results by using GWO, GBO, and IGWO-Scenario (II): 4 mm

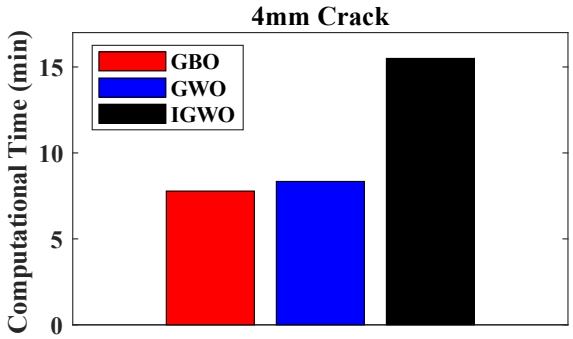

Figure 20. The computation time of 4 mm crack identification based on GWO, GBO, and IGWO-Scenario (II)

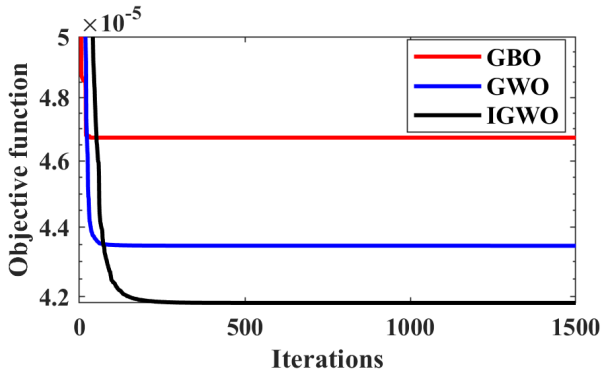

Figure 21. The convergence curves of the objective function values-Scenario (III): 6 mm

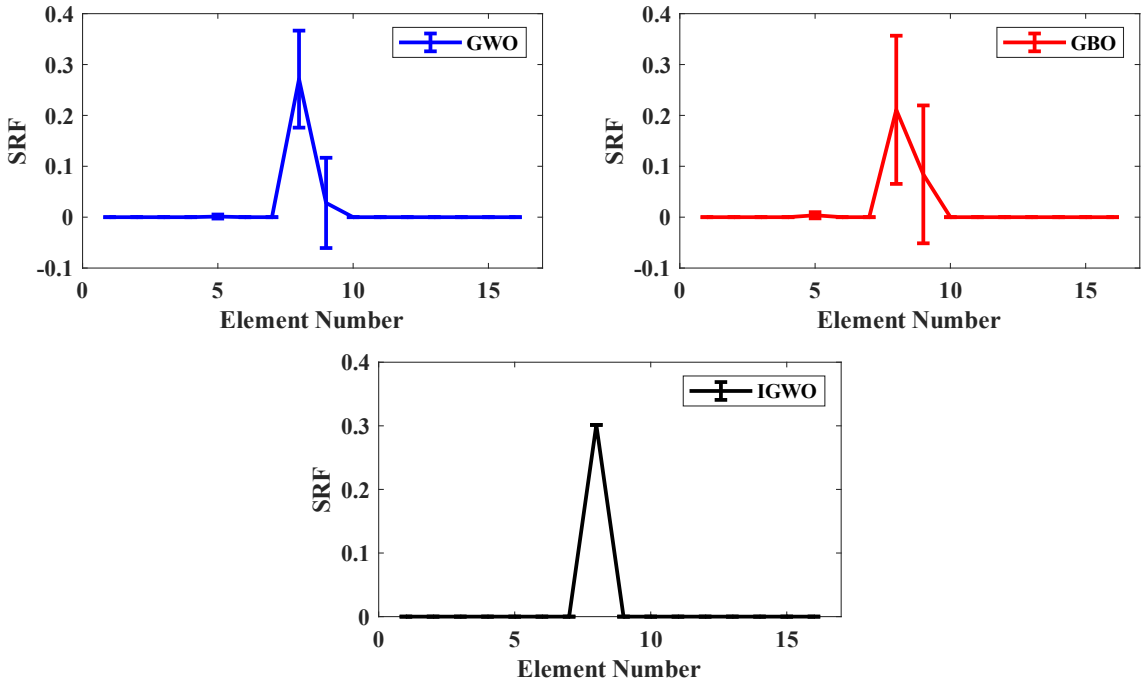

Figure 22. Identified results by using GWO, GBO, and IGWO-Scenario (III): 6 mm

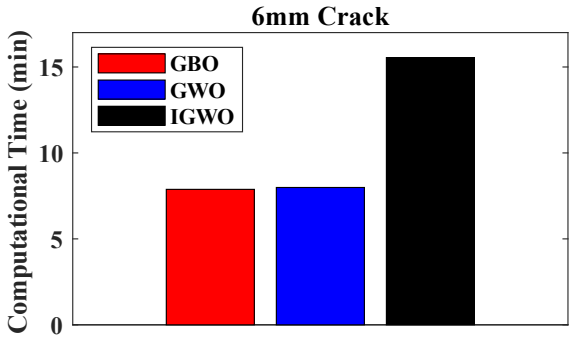

Figure 23. The computation time of 6 mm crack identification based on GWO, GBO, and IGWO-Scenario (III)

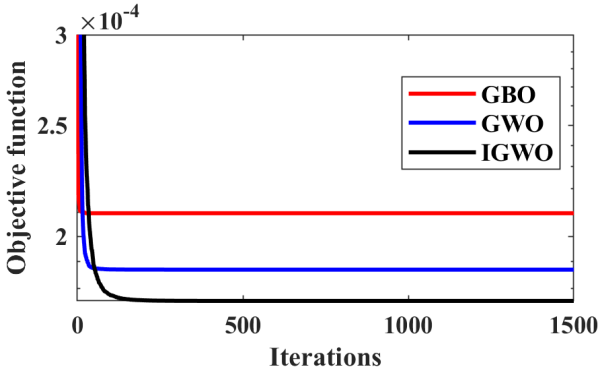

Figure 24. The convergence curves of the objective function values-Scenario (IV): 8 mm

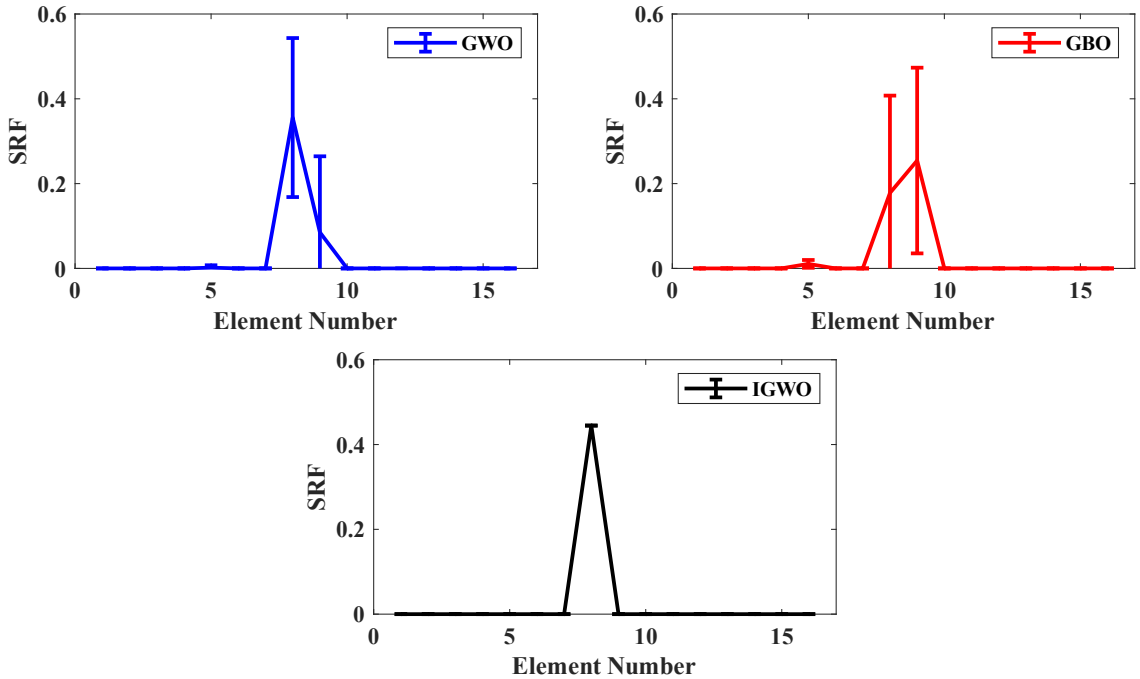

Figure 25. Identified results by using GWO, GBO, and IGWO-Scenario (IV): 8 mm

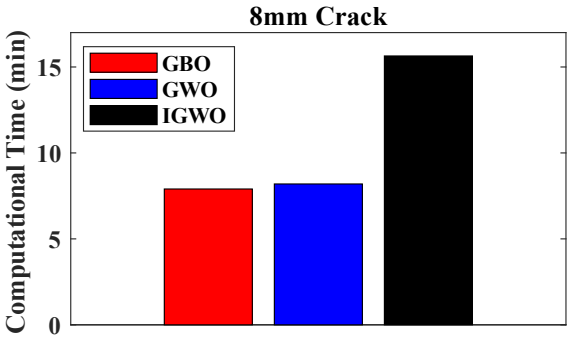

Figure 26. The computation time of 8 mm crack identification based on GWO, GBO, and IGWO-Scenario (IV)

Table 9. The performance of objective functions and optimization algorithms when considering two types of beam elements for FEM updating

Type of beam element	GWO-MTMAC	IGWO-MTMAC	GBO-MTMAC	GWO-Frequency	IGWO-Frequency	GBO-Frequency
Euler-Bernoulli beam element	•	•	•	•	•	•
Semi-rigidly connected frame element (S-RCFE)	✓	✓	•	•	•	•

Table 10. The performance of optimization algorithms for crack identification in different scenarios

Scenario	GWO-Frequency	IGWO-Frequency	GBO-Frequency
(I)	•	✓	✓
(II)	✓	✓	✓
(III)	•	✓	•
(IV)	•	✓	•

6. Conclusions

This paper applies the semi-rigidly connected frame element (S-RCFE) instead of the Euler-Bernoulli beam element to create the free-free beam's finite element model (FEM). The proposed method is employed optimization algorithms to minimize the objective function and calibrate the numerical model by adjusting the unknown parameters. Therefore, the sensitivity of three optimization algorithms, viz, grey wolf optimizer (GWO), gradient-based optimization (GBO) and an improved version of GWO (IGWO), and two objective functions based on modified total modal assurance criterion (MTMAC) and changes in natural frequency is investigated. The following results are obtained for optimization-based FEM updating when considering the S-RCFE and Euler-Bernoulli beam element:

I) Regardless of optimization technique and objective function, there are significant

disparities between experimental and updated natural frequencies when applying the Euler-Bernoulli beam element.

II) When using the S-RCFE, GWO-MTMAC and IGWO-MTMAC provide reliable and accurate results in FEM updating. However, GBO-MTMAC could not obtain a satisfactory agreement between all experimental and updated natural frequencies, and approximately 1.24% error is observed in the fourth mode.

III) When using the S-RCFE and objective function based on natural frequency changes, no strong correlation exists between updated and experimental mode shapes, regardless of optimization algorithms.

The following results are obtained for damage identification when using the updated model based on S-RCFE, an objective function relying on changes in natural frequency and three optimization algorithms:

I) The IGWO provides the most accurate and reliable results among two other algorithms.

II) The GBO competes efficiently with a lower computation time than IGWO in crack scenarios (I) and (II).

III) The GWO could function properly only for crack scenario (II).

IV) Overall, IGWO is the optimization algorithm that works perfectly to identify the crack in whole scenarios. In contrast to GWO and GBO, IGWO requires more computation time.

7. Future directions

The proposed approach based on S-RCFE and optimization algorithms should be examined under real measurement conditions and extended to other structures, such as simply supported beams, frames, pipelines, and full-scale bridges. More investigations on this method are currently underway and will be discussed in subsequent publications.

Data availability

The experimental dataset used in this study is available online.

Acknowledgments

The authors would like to thank the honorable reviewers for their insightful and valuable suggestions that substantially enhanced the paper.

Abbreviations

FEM	Finite element model
S-RCFE	Semi-rigidly connected frame element
MAC	Modal assurance criterion
MTMAC	Modified total modal assurance criterion
GWO	Grey wolf optimizer
IGWO	Improved GWO
GBO	Gradient-based optimization
SHM	Structural health monitoring
PSO	particle swarm optimization
TLBO	Teaching-learning-based optimization
IIRS	Iterated improved reduction system
DOFs	Degrees of freedom
SEREP	System equivalent reduction expansion process
ANNs	Artificial neural networks
SRF	Stiffness reduction factor
GSR	Gradient search rule
LEO	Local escaping operator

References

1. Khuc, T., et al., *A nonparametric method for identifying structural damage in bridges based on the best-fit auto-regressive models.* International Journal of Structural Stability and Dynamics, 2020. **20**(10): p. 2042012.
2. Kourehli, S., *Application of extreme learning machine to damage detection of plate-like structures.* International Journal of Structural Stability and Dynamics, 2017. **17**(07): p. 1750068.
3. Mahmoud, S., et al., *Structural response and damage evaluation of a typical highrise RC building in Dubai under an earthquake with single and multiple peaks.* Journal of Civil Engineering and Management, 2022. **28**(7): p. 509–522-509–522.
4. Le, N.T., et al., *A new method for locating and quantifying damage in beams from static deflection changes.* Engineering Structures, 2019. **180**: p. 779-792.
5. Ercolani, G., D. Felix, and N. Ortega, *Crack detection in prestressed concrete structures by measuring their natural frequencies.* Journal of Civil Structural Health Monitoring, 2018. **8**(4): p. 661-671.
6. Jayasundara, N., et al., *Locating and quantifying damage in deck type arch bridges using frequency response functions and artificial neural networks.* International Journal of Structural Stability and Dynamics, 2020. **20**(10): p. 2042010.
7. Gharehbaghi, V.R., et al., *Supervised damage and deterioration detection in building structures using an enhanced autoregressive time-series approach.* Journal of Building Engineering, 2020. **30**: p. 101292.
8. Farrar, C.R., K. Worden, and J. Dulieu-Barton, *Principles of structural degradation monitoring.* Encyclopedia of structural health monitoring, 2009.
9. Ghannadi, P., S.S. Kourehli, and S. Mirjalili, *The application of PSO in structural damage detection: An analysis of the previously released publications (2005–2020).* Frattura ed Integrità Strutturale, 2022. **16**(62): p. 460-489.
10. Pedram, M., A. Esfandiari, and M.R. Khedmati, *Frequency domain damage detection of plate and shell structures by finite element model updating.* Inverse Problems in Science and Engineering, 2018. **2** :(1)6p. 100-132.

11. Ding, Z., J. Li, and H. Hao, *Structural damage identification using improved Jaya algorithm based on sparse regularization and Bayesian inference.* Mechanical Systems and Signal Processing, 2019. **132**: p. 211-231.
12. Cao, Y. and Q. Wu ,*Optimization of control parameters in genetic algorithms: a stochastic approach.* International journal of systems science, 1999. **30**(5): p. 551-559.
13. Syafruddin, W.A., M. Köppen, and B. Benaissa. *Does the Jaya Algorithm Really Need No Parameters?* in *IJCCI*. 2018.
14. Zitar, R.A., et al., *An intensive and comprehensive overview of JAYA algorithm, its versions and applications.* Archives of Computational Methods in Engineering, 2021: p. 1-30.
15. Dhal, K.G., et al., *Effect of population size over parameter-less firefly algorithm*, in *Applications of firefly algorithm and its variants*. 2020, Springer. p. 237-266.
16. Centeno-Telleria, M., et al., *Differential evolution optimal parameters tuning with artificial neural network.* Mathematics, 2021. **9**(4): p. 427.
17. Du, D.-C., et al., *Efficiency of Jaya algorithm for solving the optimization-based structural damage identification problem based on a hybrid objective function.* Engineering Optimization, 2018. **50**(8): p. 1233-1251.
18. Khatir, S. and M.A. Wahab, *Fast simulations for solving fracture mechanics inverse problems using POD-RBF XIGA and Jaya algorithm.* Engineering Fracture Mechanics, 2019. **205**: p. 285-300.
19. Khatir, S. and M.A. Wahab, *A computational approach for crack identification in plate structures using XFEM, XIGA, PSO and Jaya algorithm.* Theoretical and Applied Fracture Mechanics, 2019. **103**: p. 102240.
20. Mohanty, B. and S. Tripathy, *A teaching learning based optimization technique for optimal location and size of DG in distribution network.* journal of electrical systems and information technology, 2016. **3**(1): p. 33-44.
21. Kundu, R.D., M. Mishra, and D. Maity, *Teaching–learning-based optimization algorithm for solving structural damage detection problem in frames via changes in vibration responses.* Architecture, Structures and Construction, 2021: p. 1-20.
22. Fallahian, S., A. Joghataie, and M.T. Kazemi, *Structural damage detection using time domain responses and Teaching-Learning-Based Optimization (TLBO) algorithm.* Scientia Iranica, 2018. **25** :(6)p. 3088-3100.
23. Shahrouzi, M. and A.-H. Sabzi, *Damage detection of truss structures by hybrid immune system and teaching–learning-based optimization.* Asian Journal of Civil Engineering, 2018. **19**(7): p. 811-825.
24. Sarmadi, H., A. Entezami, and M .Ghalehnovi, *On model-based damage detection by an enhanced sensitivity function of modal flexibility and LSMR-Tikhonov method under incomplete noisy modal data.* Engineering with Computers, 2020: p. 1-17.
25. Das, S. and N. Dhang. *Damage identification of structures using incomplete mode shape and improved TLBO-PSO with self-controlled multi-stage strategy*. in *Structures*. 2022. Elsevier.
26. Kourehli, S., *LS-SVM regression for structural damage diagnosis using the iterated improved reduction system.* International Journal of Structural Stability and Dynamics, 2016. **16**(06): p. 1550018.
27. Kourehli, S., et al., *Structural damage identification based on incomplete static responses as an optimization problem.* Scientia Iranica, 2014. **21**(4): p. 1209-1216.
28. Ghannadi, P. and S.S. Kourehli, *Investigation of the accuracy of different finite element model reduction techniques.* Structural Monitoring and Maintenance, 2018. **5**(3): p. 417-428.
29. Dinh-Cong, D., T.T. Truong, and T. Nguyen-Thoi, *A comparative study of different dynamic condensation techniques applied to multi-damage identification of FGM and FG-CNTRC plates.* Engineering with Computers, 2021: p. 1-25.
30. Dinh-Cong, D., et al., *Structural damage assessment with incomplete and noisy modal data using model reduction technique and LAPO algorithm.* Structure and Infrastructure Engineering, 2019. **15**(11): p. 1436-1449.
31. Das, S. and N. Dhang, *Damage identification of thin plates using multi-stage PSOGSA and incomplete modal data.* Applied Mathematics in Science and Engineering, 2022. **30**(1): p. 396-438.

32. Lieu, Q.X., et al., *Structural Damage Detection Using Model Order Reduction and Two-Stage Method*, in *ICSCEA 2019*. 2020, Springer. p. 1179-1187.
33. Ghannadi, P. and S.S. Kourehli, *Data-driven method of damage detection using sparse sensors installation by SEREPa.* Journal of Civil Structural Health Monitoring, 2019. **9**(4): p. 459-475.
34. Ghannadi, P. and S.S. Kourehli, *An effective method for damage assessment based on limited measured locations in skeletal structures.* Advances in Structural Engineering, 2021. **24**(1): p. 183-195.
35. Au, F., et al., *Structural damage detection based on a micro-genetic algorithm using incomplete and noisy modal test data.* Journal of Sound and Vibration, 2003. **259**(5): p. 1081-10.94
36. Ghannadi, P., et al., *Efficiency of grey wolf optimization algorithm for damage detection of skeletal structures via expanded mode shapes.* Advances in Structural Engineering, 2020. **23**(13): p. 2850-2865.
37. Abdollahi, F. and S.M. Tavakkoli, *DAMAGE IDENTIFICATION BY USING MODAL EXPANSION AND TOPOLOGY OPTIMIZATION IN THREE DIMENSIONAL ELASTICITY PROBLEMS.* International Journal of Optimization in Civil Engineering, 2019. **9**(4): p. 543-560.
38. Dinh-Cong, D., T. Nguyen-Thoi, and D.T. Nguyen, *A FE model updating technique based on SAP2000-OAPI and enhanced SOS algorithm for damage assessment of full-scale structures.* Applied Soft Computing, 2020. **89**: p. 106100.
39. Alkayem, N.F., et al., *The combined social engineering particle swarm optimization for real-world engineering problems: A case study of model-based structural health monitoring.* Applied Soft Computing, 2022. **123**: p. 108919.
40. Ghannadi, P. and S.S. Kourehli, *Structural damage detection based on MAC flexibility and frequency using moth-flame algorithm.* Structural Engineering and Mechanics, 2019. **70**(6): p. 649-659.
41. Ding, Z., R. Hou, and Y. Xia, *Structural damage identification considering uncertainties based on a Jaya algorithm with a local pattern search strategy and L0. 5 sparse regularization.* Engineering Structures, 2022. **261**: p. 114312.
42. Pahnabi, N. and S.M. Seyedpoor, *Damage identification in connections of moment frames using time domain responses and an optimization method.* Frontiers of Structural and Civil Engineering, 2021. **15** :(4)p. 851-866.
43. Tiachacht, S., et al., *Inverse problem for dynamic structural health monitoring based on slime mould algorithm.* Engineering with Computers, 2021: p. 1-24.
44. Ghannadi, P. and S.S. Kourehli, *Efficiency of the slime mould algorithm for damage detection of large-scale structures.* The Structural Design of Tall and Special Buildings, 2022: p. e1967.
45. Ghannadi, P. and S.S. Kourehli, *Multiverse optimizer for structural damage detection: Numerical study and experimental validation.* The Structural Design of Tall and Special Buildings, 2020. **29**(13): p. e1777.
46. Ghannadi, P. and S.S. Kourehli, *Model updating and damage detection in multi-story shear frames using Salp Swarm Algorithm.* Earthquakes and Structures, 2019. **17**(1): p. 63-73.
47. Tran-Ngoc, H., et al., *Damage assessment in structures using artificial neural network working and a hybrid stochastic optimization.* Scientific Reports, 2022. **12**(1): p. 1-12.
48. Nguyen-Ngoc, L., et al., *Damage detection in structures using particle swarm optimization combined with artificial neural network.* Smart Structures and Systems, 2021. **28**(1): p. 1-12.
49. Khatir, S., et al., *Improved ANN technique combined with Jaya algorithm for crack identification in plates using XIGA and experimental analysis* .Theoretical and Applied Fracture Mechanics, 2020. **107**: p. 102554.
50. Tran-Ngoc, H., et al., *An efficient artificial neural network for damage detection in bridges and beam-like structures by improving training parameters using cuckoo search algorithm.* Engineering Structures, 2019. **199**: p. 109637.
51. Khatir, S., et al., *Crack identification method in beam-like structures using changes in experimentally measured frequencies and Particle Swarm Optimization.* Comptes Rendus Mécanique, 2018. **346**(2): p. 110-12.0

52. Tran-Ngoc, H., et al., *A novel machine-learning based on the global search techniques using vectorized data for damage detection in structures.* International Journal of Engineering Science, 2020. **157**: p. 103376.
53. Khatir, S., et al., *Structural health monitoring using modal strain energy damage indicator coupled with teaching-learning-based optimization algorithm and isogoemetric analysis.* Journal of Sound and Vibration, 2019. **448**: p. 230-246.
54. Wang, D., et al., *Experimental investigation of damage identification in beam structures based on the strain statistical moment.* Advances in Structural Engineering, 2017. **20**(5): p. 747-758.
55. Chen, C. and L. Yu, *A hybrid ant lion optimizer with improved Nelder–Mead algorithm for structural damage detection by improving weighted trace lasso regularization.* Advances in Structural Engineering, 2020. **23**(3): p. 468-484.
56. Aval, S.B.B. and P. Mohebian, *Joint Damage Identification in Frame Structures by Integrating a New Damage Index with Equilibrium Optimizer Algorithm.* International Journal of Structural Stability and Dynamics, 2022. **22**(05): p. 2250056.
57. Beheshti Aval, S.B. and P. Mohebian, *Combined joint and member damage identification of skeletal structures by an improved biology migration algorithm.* Journal of Civil Structural Health Monitoring, 2020. **10**(3): p. 357-375.
58. Nanda, B., D. Maity, and D.K. Maiti, *Modal parameter based inverse approach for structural joint damage assessment using unified particle swarm optimization.* Applied Mathematics and Computation, 2014. **242**: p. 407-422.
59. Seyedpoor, S.M. and M.H. Nopour, *A two-step method for damage identification in moment frame connections using support vector machine and differential evolution algorithm.* Applied Soft Computing, 2020. **88**: p.106008 .
60. Nadimi-Shahraki, M.H., S. Taghian, and S. Mirjalili, *An improved grey wolf optimizer for solving engineering problems.* Expert Systems with Applications, 2021. **166**: p. 113917.
61. Katkhuda, H.N., H.M. Dwairi, and N. Shatarat, *System identification of steel framed structures with semi-rigid connections.* Structural engineering & mechanics, 2010. **34**(3): p. 351.
62. Ding, Z., R. Hou, and Y. Xia, *Jaya-based long short-term memory neural network for structural damage identification with consideration of measurement uncertainties.* International Journal of Structural Stability and Dynamics, 2022.
63. Cavalini Jr, A.A., et al., *Model updating of a rotating machine using the self-adaptive differential evolution algorithm.* Inverse Problems in Science and Engineering, 2016. **24**(3): p. 504-523.
64. Mashayekhi, M. and E. Santini-Bell, *Three-dimensional multiscale finite element models for in-service performance assessment of bridges.* Computer-Aided Civil and Infrastructure Engineering, 2019. **34**(5): p. 385-401.
65. Perera, R. and A. Ruiz, *A multistage FE updating procedure for damage identification in large-scale structures based on multiobjective evolutionary optimization.* Mechanical Systems and Signal Processing, 2008. **22**(4): p. 970-991.
66. Perera, R., A. Ruiz, and C. Manzano, *Performance assessment of multicriteria damage identification genetic algorithms.* Computers & Structures, 2009. **87**(1-2): p. 120-127.
67. Meruane, V. and W. Heylen, *Structural damage assessment under varying temperature conditions.* Structural Health Monitoring, 2012. **11**(3): p. 345-357.
68. Huang, M., et al., *Damage identification of bridge structures considering temperature variations-based SVM and MFO.* Journal of Aerospace Engineering, 2021. **34**(2): p. 04020113.
69. Huang, M., Y. Lei ,and S. Cheng, *Damage identification of bridge structure considering temperature variations based on particle swarm optimization-cuckoo search algorithm.* Advances in Structural Engineering, 2019. **22**(15): p. 3262-3276.
70. Kaveh, A. and A. Dadras, *Structural damage identification using an enhanced thermal exchange optimization algorithm.* Engineering Optimization, 2018. **50**(3): p. 430-451.
71. Ghiasi, R., et al., *Structural Assessment under Uncertain Parameters via the Interval Optimization Method Using the Slime Mold Algorithm.* Applied Sciences, 2022. **12**(4): p. 1876.
72. Alkayem, N.F., et al., *Inverse Analysis of Structural Damage Based on the Modal Kinetic and Strain Energies with the Novel Oppositional Unified Particle Swarm Gradient-Based Optimizer.* Applied Sciences, 2022. **12**(22): p. 11689.

73. Fan, W. and P. Qiao, *Vibration-based damage identification methods: a review and comparative study.* Structural health monitoring, 2011. **10**(1): p. 83-111.
74. Ding, Z., et al., *Improved artificial bee colony algorithm for crack identification in beam using natural frequencies only.* Inverse Problems in Science and Engineering, 2017. **25**(2): p. 218-238.
75. Mirjalili, S., S.M. Mirjalili, and A. Lewis, *Grey wolf optimizer.* Advances in engineering software, 2014. **69**: p.46-61 .
76. Ahmadianfar, I., O. Bozorg-Haddad, and X. Chu, *Gradient-based optimizer: A new metaheuristic optimization algorithm.* Information Sciences, 2020. **540**: p. 131-159.
77. Helmi, A.M., et al., *A novel hybrid gradient-based optimizer and grey wolf optimizer feature selection method for human activity recognition using smartphone sensors.* Entropy, 2021. **23**(8): p. 1065.
78. Esu, O.E., *Vibration-based indicators for damage identification in axisymmetric structures*. 2022, University of Surrey.